Scale-adaptive subgrid-scale modelling for large-eddy simulation of turbulent flows

Changping Yu, Zuoli Xiao, and Xinliang Li

Citation: Physics of Fluids **29**, 035101 (2017); doi: 10.1063/1.4977089
View online: http://dx.doi.org/10.1063/1.4977089
View Table of Contents: http://aip.scitation.org/toc/phf/29/3
Published by the American Institute of Physics

Scale-adaptive subgrid-scale modelling for large-eddy simulation of turbulent flows

Changping Yu,[1,2] Zuoli Xiao,[3,4,5,a)] and Xinliang Li[1,2]
[1]*LHD, Institute of Mechanics, Chinese Academy of Sciences, Beijing 100190, People's Republic of China*
[2]*School of Engineering Science, University of Chinese Academy of Sciences, Beijing 100049, People's Republic of China*
[3]*State Key Laboratory for Turbulence and Complex Systems, College of Engineering, Peking University, Beijing 100871, People's Republic of China*
[4]*HEDPS and Center for Applied Physics and Technology, College of Engineering, Peking University, Beijing 100871, People's Republic of China*
[5]*Beijing Innovation Center for Engineering Science and Advanced Technology, Peking University, Beijing 100871, People's Republic of China*

(Received 20 April 2016; accepted 9 February 2017; published online 13 March 2017)

The proportionality between the subgrid-scale (SGS) drain rate of kinetic energy and the viscous dissipation rate of the resolved motions is studied *a priori* by filtering a given fully resolved field and evaluating a generic form of the hypothesized energy spectrum. The ratio of the SGS drain to the resolved dissipation, on which a balance condition for the SGS dissipation across an arbitrary grid scale is founded, is shown to be independent of the turbulence Reynolds number, and can be described by a function in terms of the averaged mesh Reynolds number. Such a balance condition can serve as a physical constraint in the SGS modeling to account for the scale effects of the model coefficient(s). Scale-adaptive dynamic Smagorinsky-Lilly model and mixed nonlinear model are formulated for large-eddy simulation of transitional and/or turbulent flows in such a way that the constraint is satisfied. The newly proposed scale-adaptive dynamic SGS models are validated in simulations of homogeneous isotropic turbulence and turbulent channel flow, and prove to be superior over traditional dynamic SGS models. *Published by AIP Publishing.* [http://dx.doi.org/10.1063/1.4977089]

I. INTRODUCTION

The large-eddy simulation (LES) method has been widely used for studying the physical mechanism of high Reynolds number flows[1,2] and has been playing an increasingly important role in the simulation of engineering and environmental flows.[3,4] In LES, we formally solve the coarse-grained Navier-Stokes equations, in which the effects of subgrid-scale (SGS) motions need to be modeled through an unclosed SGS term. The SGS closure issues are of both fundamental and practical importance and have been the subject of extensive research.[5–9] More details on the SGS modeling can be found in some review articles[10–13] and the references therein. In LES, the large energy-containing eddies of turbulent motion can be directly computed, but the effect of small-scale turbulent motions (referred to as the unclosed SGS terms in the LES governing equations) is formally modeled using the resolved fields, taking into consideration that the small scales are more homogeneous and universal, and less affected by the boundary and initial conditions than the large ones. The most widely used SGS models are eddy-viscosity models, among which is the seminal Smagorinsky-Lilly (S-L) model proposed by Smagorinsky[14] and Lilly[15,16] based on dimensional arguments and the equilibrium assumption for small scales of turbulent motion. In the S-L model, the deviatoric part of the SGS stress tensor $\tau_{ij} = \widetilde{u_i u_j} - \widetilde{u}_i \widetilde{u}_j$ (namely, the anisotropic residual SGS stress tensor) is parameterized in terms of the resolved velocity field $\widetilde{u}_i$ in the following form:

$$\tau_{ij}^r \equiv \tau_{ij} - \frac{1}{3}\delta_{ij}\tau_{kk} = -2\nu_S \widetilde{S}_{ij}. \tag{1}$$

Here, the *tilde* denotes the grid filter with the filter width $\widetilde{\Delta}$, $\widetilde{S}_{ij} = \frac{1}{2}(\partial\widetilde{u}_i/\partial x_j + \partial\widetilde{u}_j/\partial x_i)$ is the resolved strain-rate tensor, and $\nu_S = C_{SL}\widetilde{\Delta}^2|\widetilde{S}|$ is the SGS eddy viscosity, with $|\widetilde{S}| = (2\widetilde{S}_{ij}\widetilde{S}_{ij})^{1/2}$ being the magnitude of the resolved strain-rate tensor (or the so-called strain scalar). Note that the model coefficient C_{SL} is the square of the original Smagorinsky constant C_S.[14] Lilly[16] evaluated the S-L model for high-Reynolds-number turbulence, assuming that $\widetilde{\Delta}$ falls in the inertial subrange, in which the sub-grid drain $\varepsilon_S = \langle \nu_S |\widetilde{S}|^2 \rangle$ is balanced by the total dissipation ε and the Kolmogorov energy spectrum $E(\kappa) = C_K \varepsilon^{2/3}\kappa^{-5/3}$ (with κ being the wavenumber) is precisely achieved. Here, the *angle brackets* denote a volume average. The model coefficient C_{SL} can be directly determined from this energy dissipation balance for a specified value of C_K.

Despite its limited success in LES of particular flows, e.g., isotropic turbulence, it is argued that the S-L model does not perform as well in the simulation of turbulent shear flows unless the Smagorinsky constant C_S is reduced by a proper factor.[1,17] For wall-bounded turbulent flows (e.g., plane channel flow), Moin and Kim[18] suggested that the Van Driest damping function[19] should be introduced in addition to the reduced

a)Author to whom correspondence should be addressed. Electronic mail: z.xiao@pku.edu.cn

C_S in order to account for the attenuation of the small-scale turbulence near the wall.

An evolutionary scenario for SGS modeling of wall-bounded flows is the so-called dynamic model proposed by Germano *et al.*[20] In the dynamic SGS models, the model coefficients, which can differ not only from flow to flow but within a single flow geometry, are determined dynamically as the numerical simulation progresses rather than given in an *a priori* or *empirical* fashion. Applying a test filter (denoted by *an overbar*) at a second scale, $\overline{\widetilde{\Delta}} = \zeta\widetilde{\Delta}$ ($\zeta \geq 1$), to the Navier-Stokes equations yields the subtest-scale (STS) stress tensor $T_{ij} = \overline{\widetilde{u_i}u_j} - \overline{\widetilde{u}_i}\overline{\widetilde{u}_j}$, which is related to the SGS stress tensor τ_{ij} through the Germano identity[6]

$$L_{ij} = T_{ij} - \overline{\tau}_{ij}, \tag{2}$$

where $L_{ij} \equiv \overline{\widetilde{u_i}\widetilde{u_j}} - \overline{\widetilde{u}_i}\overline{\widetilde{u}_j}$ is known as the resolved stress tensor and can be calculated directly from the resolved velocity field. Letting τ_{ij} and T_{ij} be parameterized by any given base SGS models, and assuming scale invariance of the model coefficient(s), a dynamic procedure is now mostly to minimize the mean square error introduced by the use of the SGS models in the Germano identity over directions of statistical homogeneity[20,21] or following fluid trajectories[22] to give rise to dynamic coefficient(s) rather than implemented for every individual fluid particle[23] in order to avoid large local variations in ν_T and numerical instability.[24] Applying the dynamic procedure outlined above to the calculation of the model coefficient in the S-L model (1) yields the dynamic Smagorinsky model (DSM) with C_{SL} given by

$$C_{SL} = \frac{\langle M_{ij}L_{ij}\rangle}{\langle M_{ij}M_{ij}\rangle}, \tag{3}$$

where $M_{ij} = -2\widetilde{\Delta}^2(\zeta^2|\overline{\widetilde{S}}|\overline{\widetilde{S}}_{ij} - \overline{|\widetilde{S}|\widetilde{S}}_{ij})$ and the *angle brackets* represent an average over statistically homogeneous directions or along pathlines. A particular strength of the dynamic concept of the SGS modeling is that it can be easily incorporated into the determination of coefficients of mixed models, such as dynamic mixed similarity model (DMSM)[25] and dynamic mixed nonlinear (gradient) model (DMNM),[26] which display much stronger correlation with the real stress than the Smagorinsky-Lilly type models.[12] More recently, Fauconnier and Dick[27] investigated the effects of the grid resolution on LES of homogeneous and isotropic turbulence through analytical and numerical methods, and suggested that the optimum grid resolution should satisfy the relation $\kappa_e\lambda \approx 0.27Re_\lambda^{0.36}$ (with κ_e, λ, and Re_λ being the effective wavenumber corresponding to the grid scale, Taylor microscale, and Taylor microscale Reynolds number).

On the one hand, the dynamic models (e.g., DSM) have the benefit of being self-contained (i.e., no need for a prescribed model parameter and near-wall correction) and have been applied successfully to many flows.[11,12] On the other hand, the dynamic concept (as well as the constant-coefficient S-L model) suffers from several deficiencies. One typical issue is that the model time scale is simply specified as the magnitude of the resolved strain-rate tensor. Another weakness arises from the scale invariance assumption of the SGS drain ($\varepsilon_S = \varepsilon$) and the model coefficient(s) ($C_{SL}(\overline{\widetilde{\Delta}}) = C_{SL}(\widetilde{\Delta})$), which is applicable to the Kolmogorov regime in the inertial subrange of high-Reynolds-number turbulence. However, the smallest resolved scale (i.e., the mesh size) in LES does not necessarily lie in the inertial range (e.g., near obstacle boundaries of complex flows), or no clear inertial subrange is present (e.g., transitional flows and low-Reynolds number flows). The issue of scale dependence in SGS modeling has attracted substantial concerns.[28] Voke[29] generalized Lilly's approach[16] and put forward a scale-dependent SGS model for LES at low mesh Reynolds numbers ($Re_{\widetilde{\Delta}} = \widetilde{\Delta}^2|\widetilde{S}|/\nu$, with ν being the kinematic viscosity) on the basis of the hypothesized full-range energy spectra of the form $E(\kappa) = C_K\varepsilon^{2/3}\kappa^{-5/3}f(\kappa)$. The SGS eddy viscosity (ν_S) is constructed such that the standard S-L model is recovered in the limit of high $Re_{\widetilde{\Delta}}$ with an offset, and the SGS effect vanishes in the completely resolved limit (i.e., $Re_{\widetilde{\Delta}} \to 0$). These low-Reynolds-number models have been applied to numerical studies of bypass transitional flow.[30] Meneveau and Lund[31] proposed a "bi-dynamic" model by introducing two test filters at two test scales. The model coefficient at the grid scale is determined through linear extrapolation using the coefficients obtained for the two test scales. Nevertheless, it was argued[32] for statistically stationary forced isotropic turbulence that the model coefficient calculated utilizing a dynamic procedure (3) corresponds to the test scale rather than the grid scale. Therefore, they suggested that a ratio of the test-scale to grid-scale coefficient ($\varrho(\widetilde{\Delta}) = C_{SL}(\overline{\widetilde{\Delta}})/C_{SL}(\widetilde{\Delta})$) be introduced when implementing the dynamic procedure across the transition from LES to direct numerical simulation (DNS). The dissipation-range ratio is given *a priori* in the form $\varrho(\widetilde{\Delta}) = 10^{-\chi}$, with $\chi = 3.23(Re_{\overline{\widetilde{\Delta}}}^{-0.92} - Re_{\widetilde{\Delta}}^{-0.92})$, while the model coefficient $C_{SL}(\widetilde{\Delta})$ is calculated dynamically (with the corresponding model being referred to as scale-dependent dynamic Smagorinsky model (SDDSM) in this paper). With a power-law assumption for the model coefficient (i.e., $C_{SL}(\widetilde{\Delta}) \sim \Delta^{\phi}$) and an introduction of a second test filter, Porté-Agel, Meneveau, and Parlange[4] generalized Meneveau and Lund's work and proposed an improved scale-dependent dynamic Smagorinsky model (ISDDSM), which allows both the ratio $\varrho(\widetilde{\Delta})$ and the coefficient $C_{SL}(\widetilde{\Delta})$ to be determined dynamically. This approach was successfully applied to the LES of a neutral atmospheric boundary layer, for which the grid scale approaches the local integral scale of the flow near the wall. The ISDDSM shows significant improvement in the predictions of the velocity spectra and mean velocity profiles as compared with the standard Smagorinsky and dynamic Smagorinsky models. Recognizing the limitations in the use of ISDDSM to rather simple flow geometries (due to the requirement for average over homogeneous directions), Bou-Zeid, Meneveau, and Parlange[33] suggested that the model coefficient be evaluated using the time-weighted average over pathlines and put forward a scale-dependent Lagrangian dynamic model for LES of practical flows in complex geometries.

The inclusion of a relationship between the test-scale and grid-scale coefficients in the dynamic procedure, as suggested by Meneveau and Lund[32] and Porté-Agel, Meneveau, and Parlange,[4] is equivalent to solving a constrained variational problem, and is consistent with the conclusion drawn by Meneveau[34] that specific balance conditions (such as the momentum

flux, and the energy flux) should be satisfied for SGS modeling in order to simulate the SGS effect more accurately. Shi, Xiao, and Chen,[35] for example, formulated a dynamic mixed SGS model under the constraint on energy fluxes across two scales. An extension of such constraint concept was then carried out to model the SGS stress for LES of helical turbulence.[36,37] Chen *et al.*[38] argued that the mean SGS stress tensor needs to be constrained by external Reynolds stress in the near-wall region towards SGS modeling for LES of wall-bounded flows. Simulation results manifest that the improvement of the constrained large-eddy simulation (CLES) methods relative to traditional LES methods is encouraging. In a recent survey article, Meneveau[39] restated the famous Germano identity in a generalized fashion that the sum of resolved and modeled SGS contributions to any quantity of physical interest should be scale-independent. The "generalized Germano identity" acts as a constraint on the model parameters to be determined during simulation.

This paper intends to address a novel methodological approach to the exploration of scale-adaptive SGS models for LES of flows at various Reynolds numbers. In this methodology, functional forms of the ratio of the SGS to resolved dissipations are obtained using DNS and hypothesized spectrum, respectively, and serve as the physical constraints to optimize the model parameters in the dynamic procedure. The rest of this paper is organized as follows. In Sec. II, a generalized constraint on the SGS dissipation is introduced on the basis of the relationship between the SGS and resolved dissipations. Furthermore, the scale-adaptive SGS models are derived in Sec. III. Then, the proposed models are validated and tested in simulations of homogeneous isotropic turbulence and turbulent channel flow in Sec. IV. Finally, the summary and concluding remarks are given in Sec. V.

II. A GENERALIZED CONSTRAINT ON THE SGS DISSIPATION

In the original Smagorinsky-Lilly model, as mentioned above, the SGS dissipation ε_S is simply assumed to equal the total dissipation ε. In reality, however, the total dissipation ε will not be known *a priori*, or might be difficult to identify *a posteriori*. Therefore, it is hypothesized that the SGS dissipation can be uniquely determined based on the resolved viscous dissipation (denoted by $\varepsilon_R = 2\nu\langle\widetilde{S}_{ij}\widetilde{S}_{ij}\rangle$). Formally, a simple proportionality between ε_S and ε_R is put forward in the form

$$\varepsilon_S = \gamma_{\widetilde{\Delta}}\varepsilon_R, \tag{4}$$

where $\gamma_{\widetilde{\Delta}}$ might differ from flow to flow, and should vary with the cutoff scale (or the grid width in LES) $\widetilde{\Delta}$. If the assumption (4) proves to be true, it can be used as an effective constraint to control the SGS dissipation when modeling the SGS stress.

For homogeneous isotropic turbulence, it is easy to show that the total dissipation rate ε in physical space can be related to the energy spectrum tensor as follows:

$$\begin{aligned}\varepsilon &= \langle 2\nu S_{ij}S_{ij}\rangle = \langle \nu|S|^2\rangle = -\langle \nu u_i\nabla^2 u_i\rangle = -\nu\lim_{r\to 0}\frac{\partial^2}{\partial r_j r_j}R_{ii}(\mathbf{r})\\ &= -\nu\lim_{r\to 0}\sum_{\kappa=0}^{\kappa_{max}} e^{i\boldsymbol{\kappa}\cdot\mathbf{r}}(-\kappa_j\kappa_j)\hat{R}_{ii}(\kappa) = \sum_{\kappa=0}^{\kappa_{max}} 2\nu\kappa^2 E(\kappa).\end{aligned} \tag{5}$$

Here, $R_{ii}(\mathbf{r}) = \langle u_i(\mathbf{x})u_i(\mathbf{x}+\mathbf{r})\rangle$ and $\hat{R}_{ii}(\kappa) = \langle \hat{u}_i^*(\kappa)\hat{u}_i(\kappa)\rangle = 2E(\kappa)$ are the two-point velocity correlation and its Fourier coefficients. Accordingly, the resolved dissipation rate ε_R can be calculated in a similar way based on a sharp spectral cutoff filter (with the cutoff wavenumber $\kappa_c = \pi/\widetilde{\Delta}$), i.e.,

$$\begin{aligned}\varepsilon_R &= \langle 2\nu\widetilde{S}_{ij}\widetilde{S}_{ij}\rangle = \langle \nu|\widetilde{S}|^2\rangle = -\langle \nu\widetilde{u}_i\nabla^2\widetilde{u}_i\rangle\\ &= -\nu\lim_{r\to 0}\frac{\partial^2}{\partial r_j r_j}\widetilde{R}_{ii}(\mathbf{r}) = -\nu\lim_{r\to 0}\sum_{\kappa=0}^{\kappa_c} e^{i\boldsymbol{\kappa}\cdot\mathbf{r}}(-\kappa_j\kappa_j)\hat{R}_{ii}(\kappa)\\ &= \sum_{\kappa=0}^{\kappa_c} 2\nu\kappa^2 E(\kappa).\end{aligned} \tag{6}$$

If one decomposes the total dissipation rate as

$$\varepsilon = \sum_{\kappa=0}^{\kappa_{max}} 2\nu\kappa^2 E(\kappa) = \sum_{\kappa=0}^{\kappa_c} 2\nu\kappa^2 E(\kappa) + \sum_{\kappa=\kappa_c}^{\kappa_{max}} 2\nu\kappa^2 E(\kappa), \tag{7}$$

the subgrid-scale dissipation is given by $\varepsilon_S = \sum_{\kappa=\kappa_c}^{\kappa_{max}} 2\nu\kappa^2 E(\kappa)$. More detailed derivations can be found in the reference book by Pope.[40] Such a full-spectrum analysis of turbulence yields the following relation:

$$\varepsilon = \varepsilon_S + \varepsilon_R. \tag{8}$$

Thus, the resolved dissipation is related to the total dissipation via

$$\frac{\varepsilon_R}{\varepsilon} = (1+\gamma_{\widetilde{\Delta}})^{-1}. \tag{9}$$

In order to ascertain the validity of the scale-dependence of the dissipation ratio function $\gamma_{\widetilde{\Delta}}$, we consider the dimensionless variable $\widetilde{\Delta}/\eta$, which can be rewritten as

$$\begin{aligned}\frac{\widetilde{\Delta}}{\eta} = \pi\frac{\kappa_d}{\kappa_c} = \widetilde{\Delta}\left(\frac{\nu^3}{\varepsilon}\right)^{-1/4} &= \widetilde{\Delta}\left(\frac{\nu^3\cdot 2\nu\langle\widetilde{S}_{ij}\widetilde{S}_{ij}\rangle}{2\nu\langle\widetilde{S}_{ij}\widetilde{S}_{ij}\rangle\varepsilon}\right)^{-1/4}\\ &= \frac{\widetilde{\Delta}(2\langle\widetilde{S}_{ij}\widetilde{S}_{ij}\rangle)^{1/4}}{\nu^{1/2}}\left(\frac{\varepsilon}{\varepsilon_R}\right)^{1/4}\\ &= \left[Re_{\widetilde{\Delta}}(1+\gamma_{\widetilde{\Delta}})^{1/2}\right]^{1/2},\end{aligned} \tag{10}$$

with $\eta = (\nu^3/\varepsilon)^{1/4}$ being the Kolmogorov length scale, $\kappa_d = 1/\eta$ the dissipation wavenumber, and $Re_{\widetilde{\Delta}}$ the mesh Reynolds number as defined by Voke.[29] Hence, it is inferred that the ratio function $\gamma_{\widetilde{\Delta}}$ can be uniquely expressed in terms of $\widetilde{\Delta}/\eta$ or $Re_{\widetilde{\Delta}}$ as long as the mesh Reynolds number is only a function of $\widetilde{\Delta}/\eta$. This argument is subject to further verification.

A. Dissipation constraint based on a model spectrum

Kovasznay[41] proposed an instructive energy spectrum in the form

$$E(\kappa) = C_K\varepsilon^{2/3}\kappa^{-5/3}\left[1-\frac{C_K}{2}\left(\frac{\kappa}{\kappa_d}\right)^{4/3}\right]^2. \tag{11}$$

Although the Kovasznay spectrum only provides the density distribution of energy up to $\kappa = (2/C_K)^{3/4}\kappa_d$, it describes one possible scenario for the energy dynamics in both inertial and dissipative ranges of the wavenumber κ. Therefore, the use of the Kovasznay spectrum as a model for the subsequent derivation does not lose any generality.

By using the Kovasznay spectrum, we can write the resolved dissipation (at scale $\widetilde{\Delta}$) as

$$\varepsilon_R = 2\nu\int_0^{\kappa_c}\kappa^2 E(\kappa)\mathrm{d}\kappa = \nu\kappa_d^{4/3}\varepsilon^{2/3}\left\{1-\left[1-\frac{C_K}{2}\left(\frac{\kappa_c}{\kappa_d}\right)^{4/3}\right]^3\right\}. \tag{12}$$

Note that the Kovasznay spectrum vanishes at $\kappa = (2/C_K)^{3/4}\kappa_d$ and $\kappa_d = 1/\eta = (\varepsilon/\nu^3)^{1/4}$. Therefore, ε_R as calculated in Eq. (12) recovers the full dissipation ε if κ_c is set to $(2/C_K)^{3/4}\kappa_d$ (the maximum wavenumber for the Kovasznay spectrum). An inspection of Eq. (10) shows that $\kappa_c/\kappa_d = \pi[Re_{\widetilde{\Delta}}(1+\gamma_{\widetilde{\Delta}})^{1/2}]^{-1/2}$. Thus, substituting for k_d and κ_c/κ_d in (12) yields

$$\frac{\varepsilon_R}{\varepsilon} = 1-\left[1-\frac{C_K}{2}\pi^{4/3}Re_{\widetilde{\Delta}}^{-2/3}\left(1+\gamma_{\widetilde{\Delta}}\right)^{-1/3}\right]^3. \tag{13}$$

Equating the right hand sides of (9) and (13) leads to

$$\gamma_{\widetilde{\Delta}} = \frac{1}{8}\left[\frac{C_K}{2}\pi^{4/3}Re_{\widetilde{\Delta}}^{-2/3}+\left(\frac{32-C_K^3\pi^4Re_{\widetilde{\Delta}}^{-2}}{12C_K\pi^{4/3}Re_{\widetilde{\Delta}}^{-2/3}}\right)^{1/2}\right]^3-1. \tag{14}$$

This demonstrates the conjecture that the SGS dissipation can be measured through the resolved dissipation modulated by a ratio coefficient $\gamma_{\widetilde{\Delta}}$, which is a function of the mesh Reynolds number $Re_{\widetilde{\Delta}}$, at least for the Kovasznay-type spectra. An inspection of (14) and (10) suggests that the ratio function $\gamma_{\widetilde{\Delta}}$ can also be expressed in terms of the dimensionless filter width $\widetilde{\Delta}/\eta$.

It shall be stressed that the above derivation is based on a low-pass sharp cutoff filter. It is anticipated that other commonly used filter functions will give similar results. As an example, we now use the Gaussian filter for noise reduction. The resolved dissipation at scale $\widetilde{\Delta}$ is then given by

$$\begin{aligned}\varepsilon_R = 2\nu\int_0^{\kappa_c}\kappa^2\widehat{G}^2E(\kappa)\mathrm{d}\kappa = \nu\kappa_d^{4/3}\varepsilon^{2/3}\Bigg\{&\left[486^{1/3}\Gamma\left(\frac{5}{3}\right)-12^{2/3}\Gamma\left(\frac{2}{3},\frac{\pi^2}{12}\right)\right]C_K\pi^{-4/3}\left(\frac{\kappa_c}{\kappa_d}\right)^{4/3}\\&+\left[12^{4/3}\Gamma\left(\frac{4}{3},\frac{\pi^2}{12}\right)-4374^{1/3}\Gamma\left(\frac{7}{3}\right)\right]C_K^2\pi^{-8/3}\left(\frac{\kappa_c}{\kappa_d}\right)^{8/3}\\&+\left[36-\left(36+3\pi^2\right)\exp\left(-\frac{\pi^2}{12}\right)\right]C_K^3\pi^{-4}\left(\frac{\kappa_c}{\kappa_d}\right)^4\Bigg\},\end{aligned} \tag{15}$$

where $\widehat{G} = \widehat{G}(\kappa,\widetilde{\Delta}) = \exp(-\kappa^2\widetilde{\Delta}^2/24) = \exp[-\pi^2(\kappa/\kappa_c)^2/24]$ is the Gaussian filter kernel in spectral space, $\Gamma(\xi) = \int_0^\infty t^{\xi-1}e^{-t}\mathrm{d}t$ is the gamma function, and $\Gamma(\xi,x) = \int_x^\infty t^{\xi-1}e^{-t}\mathrm{d}t$ is the upper incomplete gamma function. It must be mentioned that the resolved dissipation ε_R as calculated in Eq. (15) cannot recover the full dissipation ε when κ_c is set to the maximum wavenumber $(2/C_K)^{3/4}\kappa_d$, but underestimates it by about 11%. Such discrepancy is ascribed to the global damping property of the Gaussian filter. For a filter width with $\kappa_c < (2/C_K)^{3/4}\kappa_d$, however, Eq. (15) essentially yields the resolved dissipation based on a truncated Gaussian filter. Note that the upper limit of the integral is κ_c instead of the maximum wavenumber. It is shown by algebraic calculations that such simplification can result in an underprediction of the resolved dissipation by up to 25% depending on the filter width. Although Eq. (15) indeed underestimates the resolved dissipation, it can be calibrated by a correction factor α in order for it to be used in the scale-dependent SGS modeling. The simplest form of the correction factor is a constant, e.g., $\alpha \approx 0.89\cdot 0.80 = 0.71$.

It is easy to show from Eqs. (15) and (10) that the ratio of the modified ε_R to the total dissipation reads

$$\begin{aligned}\frac{\varepsilon_R}{\varepsilon} = \frac{1}{\alpha}\Big[&5.1149C_KRe_{\widetilde{\Delta}}^{-2/3}\left(1+\gamma_{\widetilde{\Delta}}\right)^{-1/3}\\&-10.1770C_K^2Re_{\widetilde{\Delta}}^{-4/3}\left(1+\gamma_{\widetilde{\Delta}}\right)^{-2/3}\\&+7.1750C_K^3Re_{\widetilde{\Delta}}^{-2}\left(1+\gamma_{\widetilde{\Delta}}\right)^{-1}\Big].\end{aligned} \tag{16}$$

By equating the right hand sides of Eqs. (9) and (16), we arrive at the solution for $\gamma_{\widetilde{\Delta}}$ in the form

$$\begin{aligned}\gamma_{\widetilde{\Delta}} = \Big[&0.99C_KRe_{\widetilde{\Delta}}^{-2/3}+0.098\Big(20.46\alpha C_K^{-1}Re_{\widetilde{\Delta}}^{2/3}\\&-43.23C_K^2Re_{\widetilde{\Delta}}^{-4/3}\Big)^{1/2}\Big]^3-1.\end{aligned} \tag{17}$$

Both Eqs. (14) and (17) can be problematic when the mesh Reynolds number $Re_{\widetilde{\Delta}}$ approaches zero, because small $Re_{\widetilde{\Delta}}$ will result in negative dissipation ratio $\gamma_{\widetilde{\Delta}}$. It is shown by algebraic calculation that $\gamma_{\widetilde{\Delta}}$ will approach zero when $Re_{\widetilde{\Delta}}$ falls down to about 7 and 19, respectively, in Eqs. (14) and (17). However, such a drawback almost has no influence on the application of these equations to the SGS modeling since the smallest mesh Reynolds number in practical LES is usually larger than these limiting values. When $Re_{\widetilde{\Delta}}$ goes to infinity, however, $\gamma_{\widetilde{\Delta}}$ calculated using both Eqs. (14) and (17) will also approach infinity, indicating that the resolved dissipation rate is negligibly small in such limit case.

It should be mentioned that the correction factor might vary in terms of the filter width ($\widetilde{\Delta}$) or the dissipation ratio ($\gamma_{\widetilde{\Delta}}$). For example, one can think of α as a function of $\gamma_{\widetilde{\Delta}}$ in the form $\alpha = \alpha_1(1+\gamma_{\widetilde{\Delta}})^{1/3}+\alpha_2$ with the coefficients $\alpha_1 = -0.028$ and $\alpha_2 = 0.92$ determined by algebraic calculation using Eq. (15).

It ought to be further stressed that the above assumptions have no specific physical reasons and the mathematical derivations are all under the conditions of statistical homogeneity and stationarity. For inhomogeneous flows, e.g., turbulent channel flow, the formulations are still applicable to homogeneous directions, i.e., the plane perpendicular to the wall-normal direction. For flows with more complex geometries, it is simply assumed that the functional dependence of $\gamma_{\widetilde{\Delta}}$ upon $Re_{\widetilde{\Delta}}$ (i.e., Eqs. (14) and (17)) remains unchanged.

B. Dissipation constraint based on data fitting

The conjecture that the ratio of the SGS dissipation to the resolved dissipation, $\gamma_{\widetilde{\Delta}}$, can be expressed as a function of the dimensionless filter width $\widetilde{\Delta}/\eta$ or the mesh Reynolds number has proven to hold for the Kovasznay spectrum using both the sharp cutoff filter and Gaussian filter. In this subsection, we intend to evaluate the validity of the conjecture based on the numerical data of three-dimensional (3D) incompressible

homogeneous isotropic turbulence (HIT). For such purpose, we have numerically solved the 3D incompressible Navier-Stokes equations in the form

$$\frac{\partial u_i}{\partial t} + \frac{\partial}{\partial x_j}(u_i u_j) = -\frac{1}{\rho}\frac{\partial p}{\partial x_i} + \nu\frac{\partial^2 u_i}{\partial x_j \partial x_j} + f_i, \qquad (18)$$

using a pseudospectral solver in a cubic box with a side length $L = 2\pi$. Periodic boundary conditions are imposed in the three directions. Here, u_i is the velocity vector and p is the pressure. The flow system is maintained statistically stationary through a large-scale forcing term f_i, which is determined dynamically in order to keep a constant energy input in the first two wavenumber shells. The dealiasing error is removed by using the Orszag's 2/3 rule.[42] The second-order Adams-Bashforth scheme is employed to perform the physical time marching. The constant energy injection rate in the first two wavenumber shells is $\varepsilon_{in} = 0.1$. The initial condition is given by a Gaussian random field with an energy spectrum of the form $E_0(\kappa) = A\kappa^2 U_0^2 \kappa_0^{-5} e^{-2\kappa^2/\kappa_0^2}$, with $\kappa_0 = 4.5786$ and $U_0 = 0.715$. A is chosen such that the initial kinetic energy is $3U_0^2/2$. More details concerning the numerical method and parameterization can be found in the article co-authored by Chen *et al.*[43] The grid resolution is 512^3, and the kinematic viscosity (ν) varies from 5×10^{-4} to 5×10^{-3}. The initial large-eddy turnover time is defined as $\tau_0 = \pi/(\kappa_0 U_0)$. The data analysis is conducted for all the flow fields obtained after five initial large-eddy turnover times when all the systems have reached a statistically steady state. The resultant Taylor microscale Reynolds numbers (Re_λ) range from 75 to 235.

The SGS dissipation rate $\varepsilon_S = -\langle\widetilde{S}_{ij}\tau_{ij}\rangle$ and resolved dissipation rate $\varepsilon_R = \langle\nu|\widetilde{S}|^2\rangle$ are calculated with varying filter width $\widetilde{\Delta}$ based on the HIT data at different Reynolds numbers. Here, a Gaussian filter function is used to remove the small-scale ($<\widetilde{\Delta}$) fluctuations. Shown in Fig. 1(a) is the inverse of the dissipation ratio, $\gamma_{\widetilde{\Delta}}^{-1}$, in terms of the dimensionless filter width $\widetilde{\Delta}/\eta$. It can be seen that all the curves (with symbols) for different Reynolds numbers nearly collapse onto each other. If we use curve-fitting method, we end up with

$$\gamma_{\widetilde{\Delta}}^{-1} = a_1(\widetilde{\Delta}/\eta)^{-3/2} + b_1(\widetilde{\Delta}/\eta)^{-7/3}, \qquad (19)$$

with $a_1 = b_1 = 30.0$ being the fitted coefficients. This implies that the dissipation ratio can be uniquely expressed as a function of $\widetilde{\Delta}/\eta$ at least for HIT with the large-scale forcing employed in this paper. The variations of the dissipation ratio, $\gamma_{\widetilde{\Delta}}$, with respect to the mesh Reynolds number are depicted in Fig. 1(b) for DNS data of HIT over a range of Reynolds numbers. The different symbols show very good agreement with each other over the entire range of mesh Reynolds numbers under consideration. A curve fitting analysis suggests that the dissipation ratio function be modeled as

$$\gamma_{\widetilde{\Delta}} = a_2\left[\ln(b_2 Re_{\widetilde{\Delta}})\right]^{27/4}, \qquad (20)$$

where $a_2 = 7\times10^{-5}$, and $b_2 = 0.7$. These numerical evidence favourably support the conjecture for $\gamma_{\widetilde{\Delta}}$ as made at the beginning of this section.

The modeled dissipation constraints (14) and (17) are also plotted in Fig. 1(b) as the dashed, dashed-dotted, and dashed-double dotted lines, respectively, for comparison. It can be seen

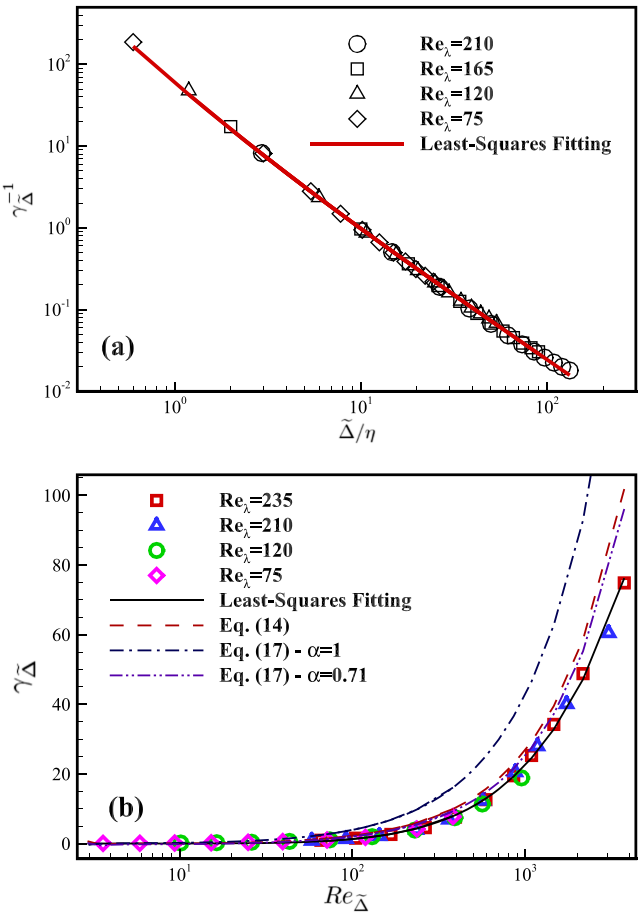

FIG. 1. (a) The inverse of the dissipation ratio, $\gamma_{\widetilde{\Delta}}^{-1}$ versus $\widetilde{\Delta}/\eta$, and (b) the dissipation ratio $\gamma_{\widetilde{\Delta}}$ versus the mesh Reynolds number $Re_{\widetilde{\Delta}}$ calculated *a priori* based on the DNS's of HIT at various Reynolds numbers (different symbols). In panel (b), the dashed line is for Eq. (14), while the dashed-dotted and dashed-double dotted lines are for Eq. (17) without and with corrections.

that the curve for Eq. (17) with $\alpha = 1$ (before correction) deviates strongly from the numerical data as discussed previously. However, the curves for Eqs. (14) and (17) with $\alpha = 0.71$ (after correction) are consistent with the numerical results very well when $Re_{\widetilde{\Delta}} < 1000$, but overestimate $\gamma_{\widetilde{\Delta}}$ when $Re_{\widetilde{\Delta}} > 1000$ in comparison with the fitted curve, which is attributed to the discrepancy between the Kovasznay spectrum and the simulated spectra in the energy-containing range, which shall be out of our interest in regard to the LES applications. It should be mentioned here that the scale-dependent formulation for the correction factor α as suggested at the end of Sec. II A yields a similar result to that using a constant value (which is not shown here in order not to pollute the data).

III. SCALE-ADAPTIVE SGS MODELS

The SGS dissipation constraint (4) based on the dissipation ratio functions (see Eqs. (14), (17), and (20)) obtained in Sec. II can be easily incorporated in the SGS modeling procedure to develop scale-adaptive SGS models for LES.

We first take the dynamic Smagorinsky model as an example, for which the deviatoric SGS stress tensor is parameterized as

$$\tau_{ij}^r = -2C_{SL}(\widetilde{\Delta})\widetilde{\Delta}^2|\widetilde{S}|\widetilde{S}_{ij}. \qquad (21)$$

Therefore, the resolved and SGS dissipation rates are given by $\varepsilon_R(\widetilde{\Delta}) = \langle \nu|\widetilde{S}|^2\rangle$ and $\varepsilon_S(\widetilde{\Delta}) = C_{SL}(\widetilde{\Delta})\widetilde{\Delta}^2\langle|\widetilde{S}|^3\rangle$, respectively. Substituting $\varepsilon_S(\widetilde{\Delta})$ and $\varepsilon_R(\widetilde{\Delta})$ into (4) yields

$$C_{SL}(\widetilde{\Delta})\widetilde{\Delta}^2\langle|\widetilde{S}|^3\rangle = \gamma_{\widetilde{\Delta}}\langle\nu|\widetilde{S}|^2\rangle. \tag{22}$$

Comparing (22) with its counterpart at the test scale $\widetilde{\overline{\Delta}} = \zeta\widetilde{\Delta}$ ($\zeta \geq 1$) leads to

$$\beta_{\widetilde{\overline{\Delta}}} = \frac{C_{SL}(\widetilde{\overline{\Delta}})\widetilde{\overline{\Delta}}^2}{C_{SL}(\widetilde{\Delta})\widetilde{\Delta}^2} = \zeta^2\frac{C_{SL}(\widetilde{\overline{\Delta}})}{C_{SL}(\widetilde{\Delta})} = \frac{\gamma_{\widetilde{\overline{\Delta}}}\langle|\widetilde{\overline{S}}|^2\rangle\langle|\widetilde{S}|^3\rangle}{\gamma_{\widetilde{\Delta}}\langle|\widetilde{S}|^2\rangle\langle|\widetilde{\overline{S}}|^3\rangle}. \tag{23}$$

Again, applying the dynamic procedure mentioned in Sec. I to the evaluation of the coefficient $C_{SL}(\widetilde{\Delta})$ in (21) yields

$$C_{SL}(\widetilde{\Delta}) = \frac{\langle R_{ij}L_{ij}\rangle}{\langle R_{ij}R_{ij}\rangle}, \tag{24}$$

where

$$R_{ij} = -2\widetilde{\Delta}^2(\beta_{\widetilde{\overline{\Delta}}}|\widetilde{\overline{S}}|\widetilde{\overline{S}}_{ij} - \overline{|\widetilde{S}|\widetilde{S}_{ij}}). \tag{25}$$

The Smagorinsky model with the coefficient identified by (24) is termed as the scale-adaptive dynamic Smagorinsky model (SADSM).

The advantage of the proposed dissipation constraint lies in that it can be easily taken into account in the construction of mixed SGS models. Here, we choose the mixed nonlinear model[44,45] to illustrate the general procedure for the inclusion of the SGS dissipation constraint (4). The general form of the mixed nonlinear model can be written as

$$\tau_{ij}^{mnl} = C_1(\widetilde{\Delta})\widetilde{\Delta}^2|\widetilde{S}|\widetilde{S}_{ij} + C_2(\widetilde{\Delta})\widetilde{\Delta}^2\widetilde{W}_{ik}\widetilde{W}_{jk}, \tag{26}$$

where $\widetilde{W}_{ik} = \partial\widetilde{u}_i/\partial x_k$ is the filtered velocity gradient tensor. This formulation in (26) benefits from the features of both the Smagorinsky-Lilly part and the tensorial eddy-viscosity part, of which, the former serves as an energy dissipation provider and is characterised by good numerical robustness and stability, and the latter is good at capturing the so-called backscatters and does not rely on a second filtering.

Note that in the traditional dynamic procedure, the model coefficients C_1 and C_2 are assumed to be scale-independent. Such assumption is a substantially stiff constraint and is valid only when the grid and test scales are within the inertial subrange. To take into account the scale effect on the two model coefficients, we need another physical constraint in addition to the SGS dissipation constraint (i.e., Eq. (4)). For simplicity, it is conjectured that the partition of the SGS dissipation between the Smagorinsky term and the nonlinear term remains unchanged at different scales. The assumption made as such is based on the fact that the Smagorinsky term provides most of the SGS dissipation in the mixed model. With this simple constraint, one can easily show that the ratio of the model coefficient at the test scale $\widetilde{\overline{\Delta}}$ to that at the grid scale $\widetilde{\Delta}$ takes the same expression as in (23), i.e.,

$$\beta_{\widetilde{\overline{\Delta}}}^{mnl} = \zeta^2\frac{C_1(\widetilde{\overline{\Delta}})}{C_1(\widetilde{\Delta})} = \zeta^2\frac{C_2(\widetilde{\overline{\Delta}})}{C_2(\widetilde{\Delta})} = \beta_{\widetilde{\overline{\Delta}}} = \frac{\gamma_{\widetilde{\overline{\Delta}}}\langle|\widetilde{\overline{S}}|^2\rangle\langle|\widetilde{S}|^3\rangle}{\gamma_{\widetilde{\Delta}}\langle|\widetilde{S}|^2\rangle\langle|\widetilde{\overline{S}}|^3\rangle}. \tag{27}$$

If we use the dynamic procedure to determine the model coefficients with the model coefficients constrained by (27), we will end up with

$$C_1(\widetilde{\Delta}) = \frac{\langle L_{ij}P_{ij}\rangle\langle Q_{ij}Q_{ij}\rangle - \langle L_{ij}Q_{ij}\rangle\langle P_{ij}Q_{ij}\rangle}{\langle P_{ij}P_{ij}\rangle\langle Q_{ij}Q_{ij}\rangle - \langle P_{ij}Q_{ij}\rangle\langle P_{ij}Q_{ij}\rangle} \tag{28}$$

and

$$C_2(\widetilde{\Delta}) = \frac{\langle L_{ij}Q_{ij}\rangle\langle P_{ij}P_{ij}\rangle - \langle L_{ij}P_{ij}\rangle\langle P_{ij}Q_{ij}\rangle}{\langle P_{ij}P_{ij}\rangle\langle Q_{ij}Q_{ij}\rangle - \langle P_{ij}Q_{ij}\rangle\langle P_{ij}Q_{ij}\rangle}, \tag{29}$$

where

$$P_{ij} = \widetilde{\Delta}^2(\beta_{\widetilde{\overline{\Delta}}}|\widetilde{\overline{S}}|\widetilde{\overline{S}}_{ij} - \overline{|\widetilde{S}|\widetilde{S}_{ij}}) \tag{30}$$

and

$$Q_{ij} = \widetilde{\Delta}^2(\beta_{\widetilde{\overline{\Delta}}}\widetilde{\overline{W}}_{ik}\widetilde{\overline{W}}_{jk} - \overline{\widetilde{W}_{ik}\widetilde{W}_{jk}}). \tag{31}$$

The mixed model (26) with the coefficients determined by (28) and (29) is referred to as the scale-adaptive dynamic mixed (nonlinear) model (SADMM).

IV. COMPUTATIONAL VALIDATION AND RESULTS

A. *A priori* test

The proposed scale-adaptive SGS models are tested *a priori* by using the DNS data of HIT obtained in Sec. II B. Similar conclusions can be drawn for all data at various Reynolds numbers. Without loss of generality, we only present the results calculated from the turbulent velocity fields at Taylor Reynolds number $Re_\lambda = 165$ ($\nu = 0.001$). For simplicity, a Gaussian filter is used to filter out the small scales of turbulent motion. The scale-adaptive dynamic Smagorinsky models with $\beta_{\widetilde{\overline{\Delta}}}$ determined by Eqs. (17) and (20) are referred to as SADSM(M) and SADSM(F), respectively. Accordingly, the scale-adaptive dynamic mixed models are named as SADMM(M) and SADMM(F), separately. In addition, the results given by the scale-dependent dynamic Smagorinsky model (SDDSM) proposed by Meneveau and Lund,[32] the traditional dynamic Smagorinsky model (DSM), and the dynamic mixed (nonlinear) model (DMM) are also presented here for the purpose of comparison.

The parameter $\beta_{\widetilde{\overline{\Delta}}}$, which serves as a constraint for the Smagorinsky model coefficients at the test and filter scales, is first evaluated when the filter width $\widetilde{\Delta}$ varies from the dissipative to inertial range of turbulence. Shown in Fig. 2 is $\beta_{\widetilde{\overline{\Delta}}}$ as a function of the mesh Reynolds number $Re_{\widetilde{\Delta}}$ as well as the normalized filter width $\widetilde{\Delta}/\eta$ for SADSM(M) and SADSM(F). Note that in traditional DSM, this constraint parameter remains constant, i.e., $\beta_{\widetilde{\overline{\Delta}}} = 4$ for given $\zeta = 2$. The corresponding result from SDDSM is also plotted for comparison. It turns out that the values for both SADSM(M) and SADSM(F) are larger than that for SDDSM, and are increasingly so in low-mesh Reynolds number range (dissipative range). All the values for different models (except DSM) decrease monotonically with increasing $Re_{\widetilde{\Delta}}$, and show a tendency to approach 4 when the mesh Reynolds number $Re_{\widetilde{\Delta}} \sim 850$, beyond which a short inertial range of turbulent motion ($70 < \widetilde{\Delta}/\eta < 100$, i.e., $900 < Re_{\widetilde{\Delta}} < 1400$ as indicated by the region between the two vertical dashed lines in Fig. 2) is achieved in this simulation case. It should be mentioned that the asymptotic value of $\beta_{\widetilde{\overline{\Delta}}}$ for SADSM(M) is also dependent on C_K, which is another

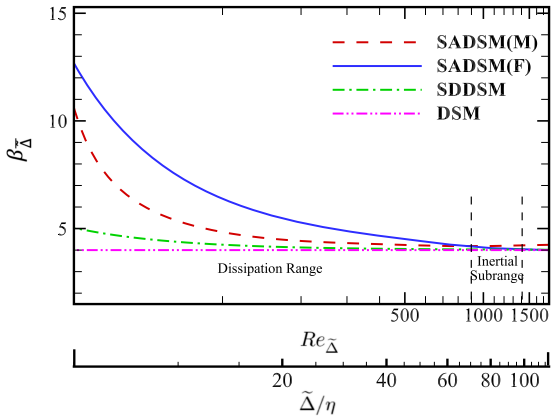

FIG. 2. The constraint for the Smagorinsky model coefficients at the test and filter scales $\beta_{\widetilde{\widetilde{\Delta}}}$ versus the mesh Reynolds number $Re_{\widetilde{\Delta}}$ and the filter width $\widetilde{\Delta}$ calculated *a priori* using the DNS data of HIT at $Re_\lambda = 165$: SADSM(M) (dashed), SADSM(F) (solid), SDDSM (dashed-dotted), and DSM (dashed-double dotted).

important parameter in (17) in addition to $Re_{\widetilde{\Delta}}$ and whose value remains controversial, especially for relatively low-Reynolds number flows. In this paper, C_K is specified as 1.6, which is within a reasonable range suggested in the experimental measurement[46] and numerical simulation[47] of turbulence. It should also be stressed that SADSM(M) does not apply in very low-mesh Reynolds number regimes (not shown in this figure) because the Kovaznay spectrum cannot model the spectral distribution of turbulent kinetic energy beyond $\kappa = (2/C_K)^{3/4}\kappa_d$ as mentioned previously. The parameter $\beta^{mnl}_{\widetilde{\widetilde{\Delta}}}$ shall take the same values as $\beta_{\widetilde{\widetilde{\Delta}}}$ as conjectured in Sec. III.

The model coefficient $C_{SL}(\widetilde{\Delta})$ in Eq. (24) is calculated based on different $\beta_{\widetilde{\Delta}}$ with various filter widths. Plotted in Fig. 3 are the variations of C_{SL} with respect to the mesh Reynolds number $Re_{\widetilde{\Delta}}$, which is associated with the grid scale of LES and can be easily obtained in computation, for different Smagorinsky-Lilly-type models, i.e., SADSM(M), SADSM(F), SDDSM, and DSM. The peak values for DSM and SDDSM are about 0.02 at $Re_{\widetilde{\Delta}} \sim 300$ around which a short plateau range is achieved in this simulation case, while the peak values for SADSM(M) and SADSM(F) are all smaller than 0.02 by 10% and 20%, respectively. Note that the former peak value is close to those obtained for the dynamic Smagorinsky model and modified dynamic model as reported in the paper by Meneveau and Lund.[32] It should be mentioned here that the discrepancy between the mesh Reynolds numbers at which DSM and SADSM(F) observe their maximum coefficients lies in the fact that the model coefficient obtained in DSM corresponds to the test-filter scale rather than the gird-filter scale.[32] As the mesh Reynolds number decreases (corresponding to the decreasing filter length), the coefficients for different models also decrease. The coefficients for SADSM(M) and SADSM(F) drop more rapidly than those for DSM and SDDSM. At large scales ($Re_{\widetilde{\Delta}} > 800$), the drops in coefficients for all models are attributed to the effects of large-scale forcing.

The mixed models with different constraints are tested *a priori* with the coefficients C_1 and C_2 determined by Eqs. (28) and (29) using the filtered DNS data at various filter widths. The calculated results are shown in Fig. 4. Note that in Fig. 4(a), $-C_1$ is presented as opposed to C_1 for the purpose of better visualization and comparison. It can be seen that the variation trends of the predicted coefficient $-C_1$ for different models are similar to those for the single-term Smagorinsky

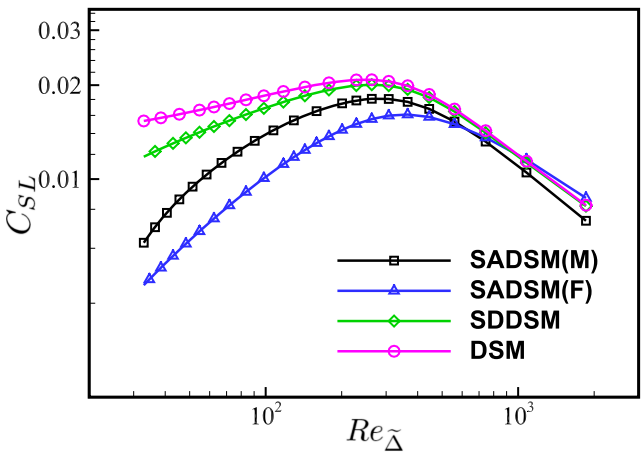

FIG. 3. The model coefficients C_{SL} calculated *a priori* at various mesh Reynolds numbers for the Smagorinsky-Lilly-type models with different constraints: SADSM(M) (line with squares), SADSM(F) (line with triangles), SDDSM (line with diamonds), and DSM (line with circles).

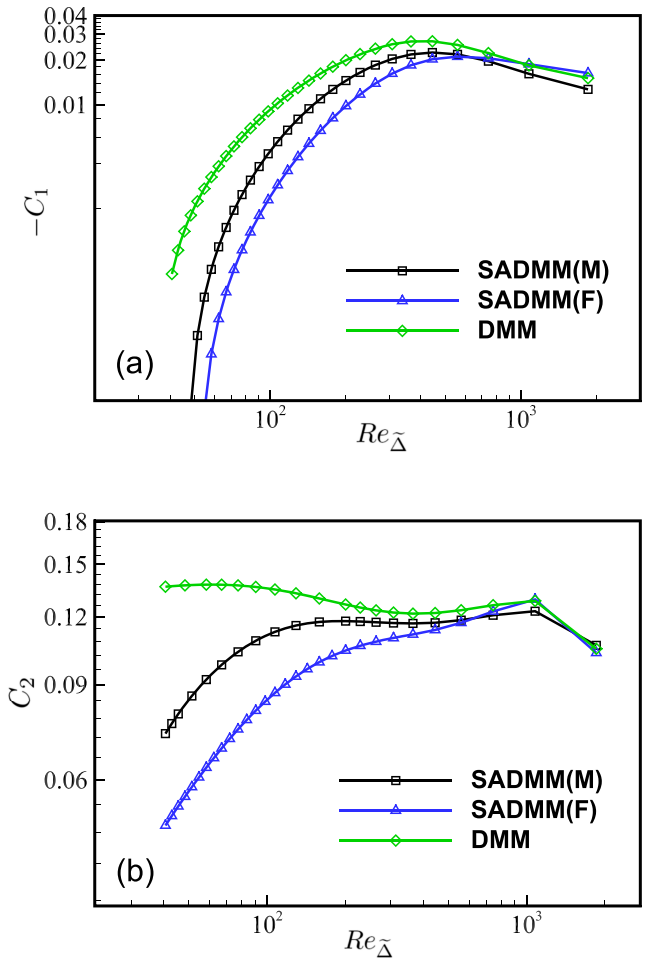

FIG. 4. The model coefficients (a) $-C_1$ and (b) C_2 calculated *a priori* at various mesh Reynolds numbers for the mixed models with different constraints: SADMM(M) (line with squares), SADMM(F) (line with triangles), and DMM (line with diamonds).

models depicted in Fig. 3, but the coefficient for SADMM(F) drops more rapidly than that for SADMM(M) at small filter scales. As seen in Fig. 4(b), nearly all the values of C_2 for SADMM(M) and SADMM(F) are smaller than that for DMM, especially at small mesh Reynolds numbers. When $\widetilde{\Delta}$ approaches the dissipative scales, C_2 for SADMM(M) and SADMM(F) shows a monotonic decrease while that for DMM yields a slight increase, which is due to the fact that the traditional dynamic procedure tends to amplify the impact of the nonlinear term in the mixed model. The proposed constraint in the present paper can effectively overcome this difficulty.

B. *A posteriori* test

1. Homogeneous and isotropic turbulence

The proposed scale-adaptive SGS models are first validated *a posteriori* in LES of the large-scale forced isotropic turbulence at various Reynolds numbers. Formally, the pseudospectral solver solves the filtered Navier-Stokes equations in the following form:

$$\frac{\partial \widetilde{u}_i}{\partial t} + \frac{\partial}{\partial x_j}(\widetilde{u}_i \widetilde{u}_j) = -\frac{1}{\rho}\frac{\partial \widetilde{p}}{\partial x_i} + \nu \frac{\partial^2 \widetilde{u}_i}{\partial x_j \partial x_j} - \frac{\partial \tau_{ij}}{\partial x_j} + \widetilde{f}_i. \quad (32)$$

Similar to the DNS, the flow system is maintained by injecting energy in the first two wavenumber shells at constant rate, which can dynamically yield the large-scale forcing $\widetilde{f}_i$. All computations are performed starting from a Gaussian random field with an energy spectrum as introduced in Sec. II B for DNS. Here, we only present the results for the low-Reynolds number case with $\nu = 0.001$. The results from DNS with the same input parameters are used for comparison purpose.

We show in Fig. 5 the energy spectra calculated in LES using different Smagorinsky-Lilly-type models, i.e., SADSM(M), SADSM(F), SDDSM, and DSM, respectively. Two spatial grid resolutions ((a) 64^3 and (b) 128^3) are chosen to demonstrate the scale-adaptive capability of the proposed model in predicting the SGS effect on the resolved motions. The long dissipative tails of the DNS spectra are truncated in order to provide a more clear comparison. The vertical dashed lines marked by different values of κ indicate the grid scales of various LES cases. In the low-resolution case (see Fig. 5(a)), for which the grid scale is approximately at the upper edge of the dissipative range, both SADSM(M) and SADSM(F) predict the spectrum more accurately than SDDSM and DSM as compared with the DNS data, especially at the upper edge of the inertial range and around the grid scale. In the high-resolution case (see Fig. 5(b)), SADSM(M) and SADSM(F) also provide improved prediction of the energy spectrum in the dissipative range in comparison with SDDSM and DSM. For example, the scale-adaptive models can improve the prediction of the near grid-scale spectrum by up to 67% as compared with DSM and SDDSM.

The low energy densities at high wavenumbers predicted by SDDSM and DSM may result from the overprediction of the model coefficient as can be clearly seen in Figs. 6(a) and 6(b), which display the time evolution of the model coefficients C_{SL} for different models on 64^3 and 128^3 grid points, respectively, as the computations progress. Note that the horizontal axis has

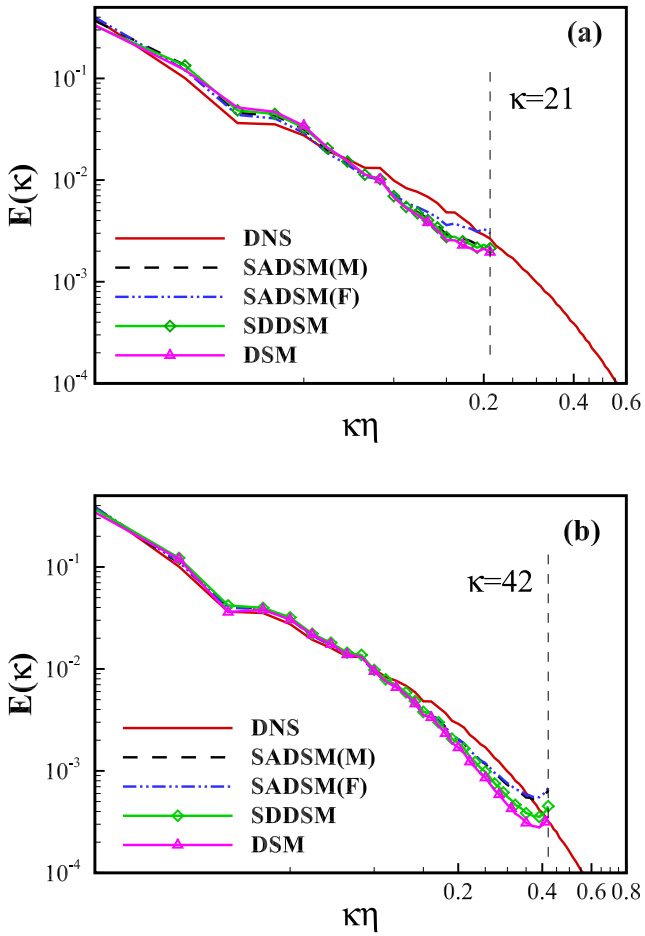

FIG. 5. Energy spectra obtained in LES of forced isotropic turbulence with spatial grid resolutions of (a) 64^3 and (b) 128^3, respectively. SADSM(M) (dashed), SADSM(F) (dashed-double dotted), SDDSM (line with diamonds), and DSM (line with triangles).

been normalized by τ_0, which is the initial large-eddy turnover time defined by the input characteristic parameters (see Sec. II B). In the low-resolution case, all the calculated model coefficients are close to each other, although the coefficients for SADSM(M) and SADSM(F) are a little bit smaller than those for SDDSM and DSM. In high-resolution case, however, there exist considerable discrepancies among the coefficients for different models. For example, the coefficient for SADSM(M) is almost 40% less than that for DSM, but is about 12% larger than that for SADSM(F). The difference between the coefficients for SADSM(M) and SADSM(F) should arise from the difference between the Kovasznay spectrum and the calculated spectra in the vicinity of grid scales.

The proposed mixed models are also implemented *a posteriori* in LES of the forced isotropic turbulence with the same input parameters as above. Depicted in Figs. 7(a) and 7(b) are the energy spectra calculated by using SADMM(M), SADMM(F), and DMM on 64^3 and 128^3 modes, respectively. Accordingly, we show in Fig. 8 the resultant model coefficients for the Smagorinsky term with a negative sign as a prefix ($-C_1$) in terms of the simulation time t/τ_0. Similarly, the time variation of the calculated model coefficients for the nonlinear term (C_2) is plotted in Fig. 9.

From Fig. 7, we can see that the scale-adaptive mixed models can provide an improvement in predicting the energy

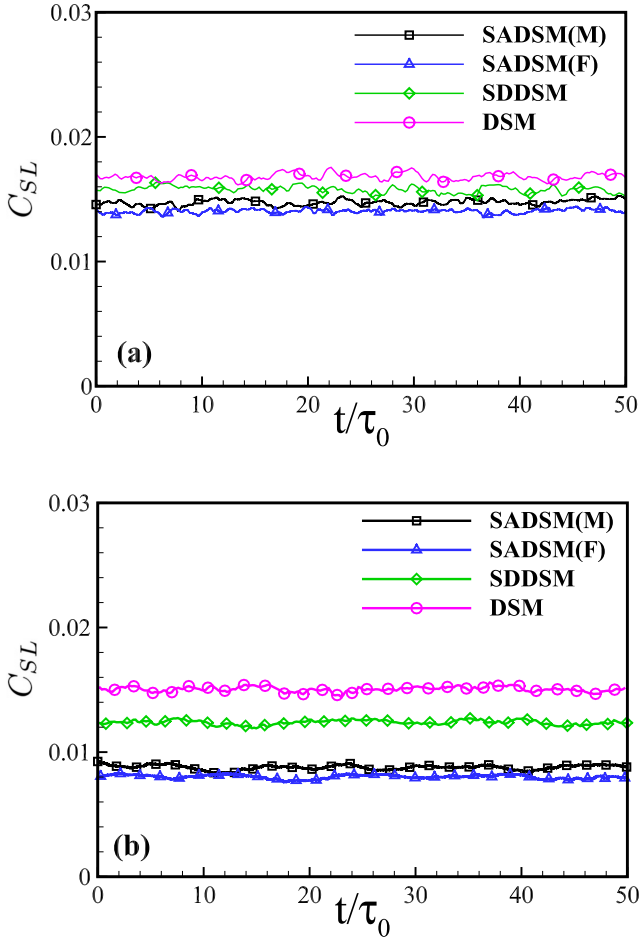

FIG. 6. Time evolution of the model coefficient C_{SL} in LES of forced isotropic turbulence with spatial grid resolutions of (a) 64^3 and (b) 128^3, respectively. SADSM(M) (line with squares), SADSM(F) (line with triangles), SDDSM (line with diamonds), and DSM (line with circles).

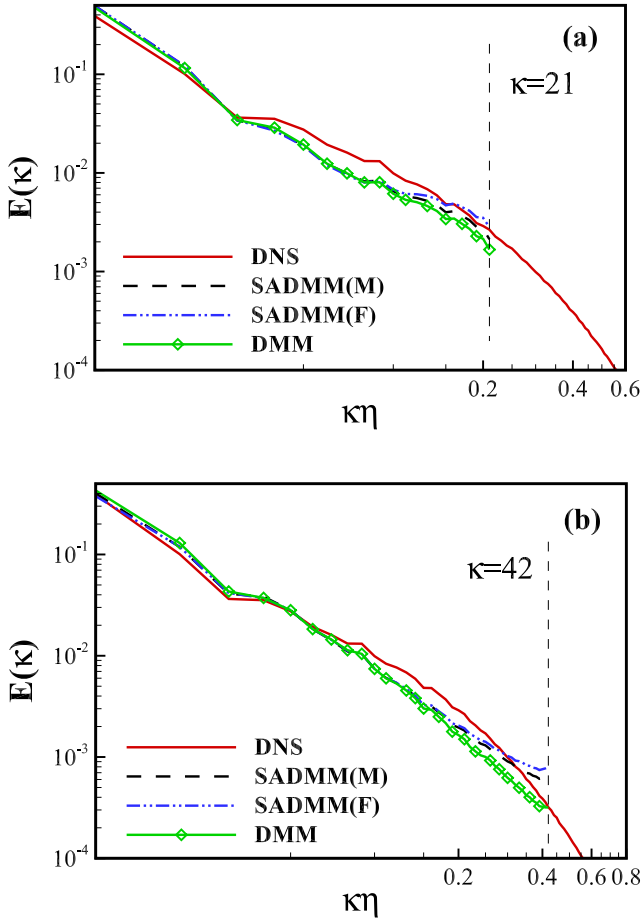

FIG. 7. Energy spectra obtained in LES of forced isotropic turbulence with spatial grid resolutions of (a) 64^3 and (b) 128^3, respectively. SADMM(M) (dashed), SADMM(F) (dashed-double dotted), and DMM (line with diamonds).

spectrum for large and grid scales. Though the mixed models can capture the lower-mode energy densities, they tend to underestimate the energy spectrum in the inertial range (see Fig. 7(a)) or in the neighbourhood of the lower edge of the inertial range (see Fig. 7(b)) when compared with the results from the single-term models (see Fig. 5) and DNS. Such performance of the mixed models can be ascribed to the compromise of the Smagorinsky term in competition with the nonlinear term since the traditional dynamic procedure (the method of least squares based on SGS stress) has a tendency to lay emphasis on the latter and attenuate the former.[9]

The inclusion of the scale-adaptive constraint for the model coefficient can not only decrease the overpredicted model coefficients but also adjust the contributions made by the two terms in a more reasonable fashion. This can be partially manifested by the model coefficients computed in LES as shown in Figs. 8 and 9. It can be seen that the model coefficients (both $-C_1$ and C_2) for the scale-adaptive models are all less than those for DMM on different grids. For DMM, $-C_1$ on 128^3 modes decreases by about 67% in comparison with that on 64^3 modes, but C_2 remains almost unchanged on different grids. For the scale-adaptive models (see SADMM(M) and SADMM(F)), however, both $-C_1$ and C_2 decrease by as high as 80% and 40%, respectively, when the grid resolution changes from 64^3 to 128^3. Therefore, the use of the scale-adaptive constraint for model coefficient can be useful in constructing a more physical and reliable multi-term SGS model, although the example employed in the present paper does not perform very well with surprising results as far as the energy spectrum is concerned.

2. Turbulent channel flow

In practical engineering applications, turbulent flows are usually subject to the influence of wall boundaries, which pose a big challenge to the SGS modeling for LES. In this section, the proposed scale-adaptive SGS models are applied to numerical simulation of turbulent channel flow for validation purposes. The filtered Navier-Stokes equations (32) are solved in a cuboid box of $4\pi\delta \times 2\delta \times 2\pi\delta$, where δ is the channel half-width. The Fourier-Chebyshev pseudospectral method[48] is employed for spatial discretization. Time integration is carried out using a semi-implicit Runge-Kutta scheme, i.e., the Crank-Nicolson scheme for the linear term, and the second-order Adams-Bashforth scheme for the nonlinear term. The three-second truncation rule[49] is used to eliminate the aliasing errors. Periodic boundary conditions are set in the streamwise and spanwise directions, and non-slip boundary conditions are assigned at the walls ($y = \pm\delta$). A constant pressure gradient in the streamwise direction is provided to drive the flow.

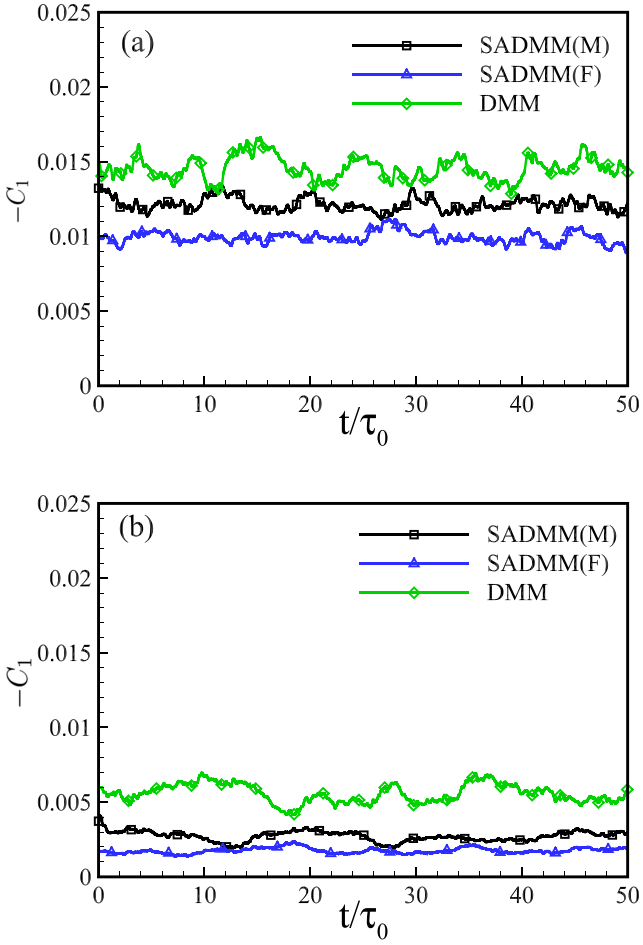

FIG. 8. Time evolution of the model coefficient $-C_1$ in LES of forced isotropic turbulence with spatial grid resolutions of (a) 64^3 and (b) 128^3, respectively. SADMM(M) (line with squares), SADMM(F) (line with triangles), and DMM (line with diamonds).

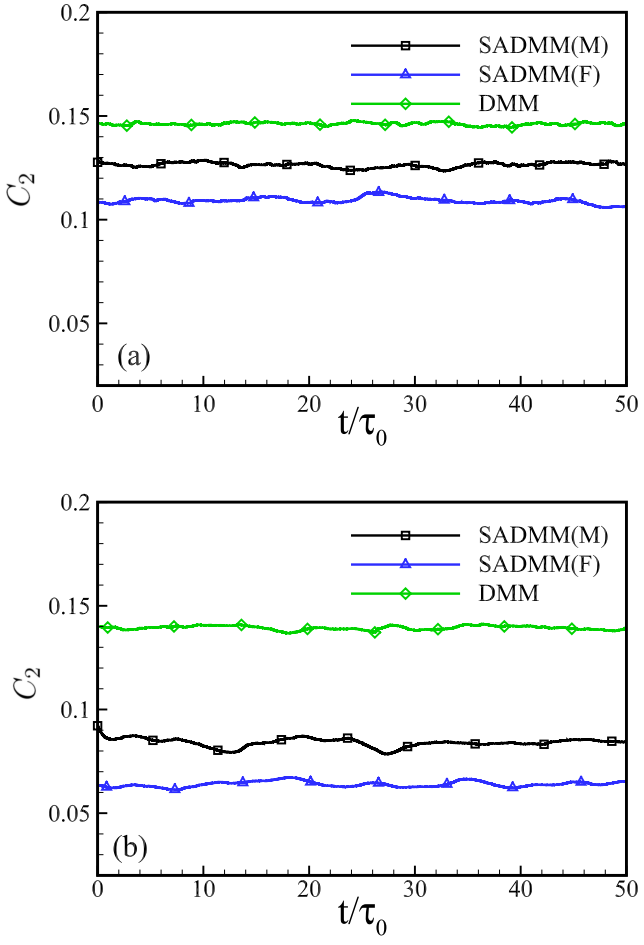

FIG. 9. Time evolution of the model coefficient C_2 in LES of forced isotropic turbulence with spatial grid resolutions of (a) 64^3 and (b) 128^3, respectively. SADMM(M) (line with squares), SADMM(F) (line with triangles), and DMM (line with diamonds).

The filtering procedure is operated in the x-z plane using a top-hat filer. The grid filter width is $\widetilde{\Delta} = [\Delta_x \Delta_z^2]^{1/3}$, and the test-filter width is taken as $\widetilde{\widetilde{\Delta}} = 2\widetilde{\Delta}$. The friction Reynolds number ($Re_\tau = u_\tau \delta/\nu$, with u_τ being the friction velocity) is prescribed as 180. Three grid resolutions, i.e., $48\times64\times48$ (GRID1), $64\times64\times64$ (GRID2), and $80\times64\times80$ (GRID3), are used for the grid-convergence study before the main results are presented. The benchmark DNS is carried out on $128\times128\times128$ grid points.

Shown in Fig. 10 are the mean velocity profiles calculated by LES using (a) SADSM(M), (b) SADSM(F), and (c) DSM at different grid resolutions. It can be seen that all three SGS models show good grid-convergence property as the grid number is larger than or equal to 64 in the streamwise and spanwise directions. The velocity profiles predicted by SADSM(M) and SADSM(F) agree with the law of the wall very well, while those predicted by DSM deviate obviously from the log-law in the outer layer with a higher intercept.

The mean velocity profiles from SADSM(M) and SADSM(F) are further compared with those from DSM and DNS as depicted in Fig. 11. Note that the LES results on GRID3 are presented here. It is clearly seen that the profiles from SADSM(M) and SADSM(F) almost collapse onto the profile from DNS. Nevertheless, the profile given by DSM lifts up in the log-law region as compared with the DNS result. Specifically, DSM overpredicts the mean velocity by up to 7%, while the maximum deviation of the results given by scale-adaptive models from the DNS benchmark data is less than 1%. Therefore, the scale-adaptive SGS models are superior to the traditional dynamic Smagorinsky model, which is based on the scale-invariance assumption, in simulating wall-bounded turbulence, especially in the near-wall regions.

Turbulence intensity is one of the most important quantities in turbulent flows. Therefore, one can assess the fidelity of an LES method through measuring the predicted turbulence intensities. We show in Fig. 12 the resolved turbulence intensities calculated in LES using SADSM(M), SADSM(F), and DSM at different grid resolutions to evaluate the scale-adaptive property of the proposed models. The DNS data are also presented for comparison purposes. It is clear to the eyes that the resolved turbulence intensities given by the scale-adaptive SGS models (SADSM(M) and SADSM(F)) are closer to the DNS data than those given by DSM for all three grid resolutions. Hence, it is inferred that the scale-adaptive SGS models suggested in this paper can predict turbulence better than traditional dynamic Smagorinsky models.

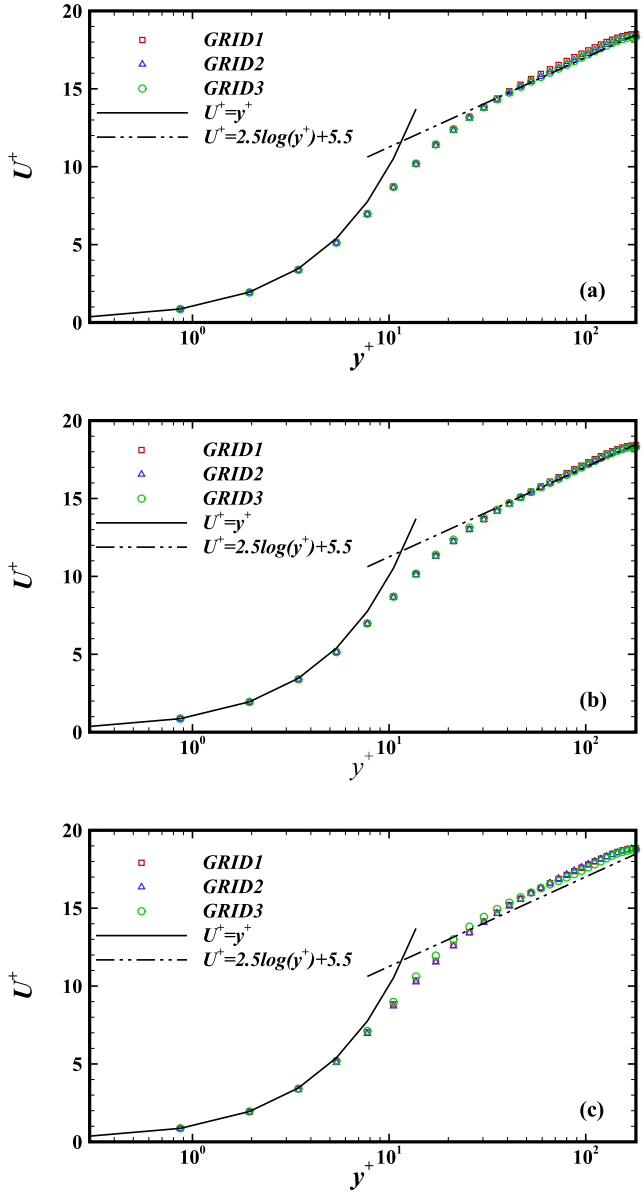

FIG. 10. Mean velocity profiles in wall units calculated in LES using (a) SADSM(M), (b) SADSM(F), and (c) DSM at different grid resolutions: GRID1 ($48 \times 64 \times 48$, squares), GRID2 ($64 \times 64 \times 64$, deltas), and GRID3 ($80 \times 64 \times 80$, circles).

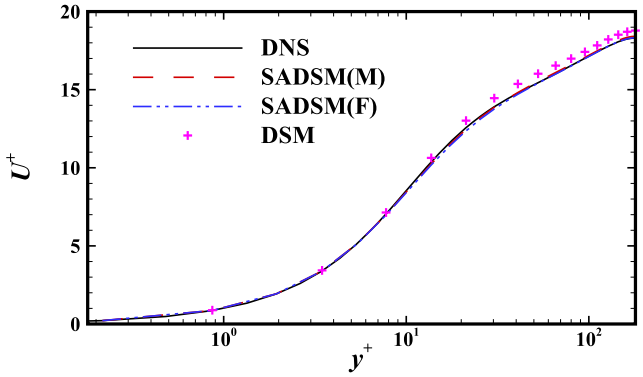

FIG. 11. Mean velocity profiles in wall units predicted by SADSM(M) (dashed line), SADSM(F) (dashed-double dotted line), and DSM (plus signs) at $80 \times 64 \times 80$ resolution. The data from DNS (solid line) are plotted for comparison.

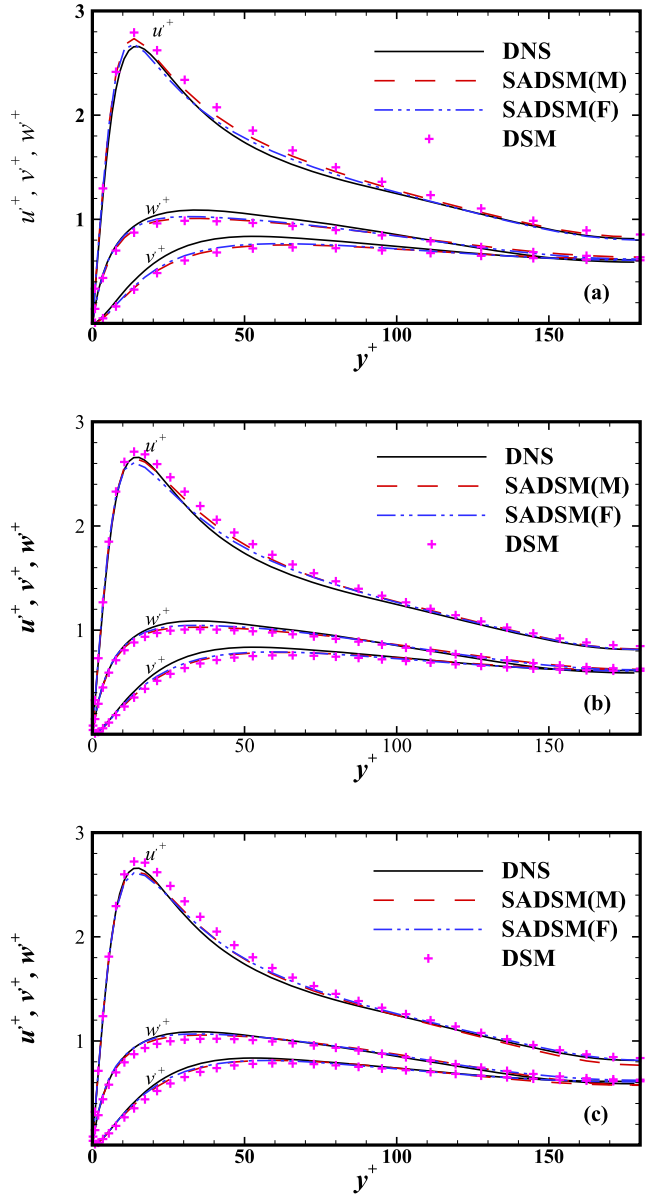

FIG. 12. Resolved turbulence intensities normalized by friction velocity from SADSM(M) (dashed line), SADSM(F) (dashed-double dotted line), and DSM (plus signs) at different grid resolutions: (a) GRID1 ($48 \times 64 \times 48$), (b) GRID2 ($64 \times 64 \times 64$), and (c) GRID3 ($80 \times 64 \times 80$). The DNS data (solid line) are also plotted for comparison.

The capability to accurately simulate the friction force, especially in the near-wall region, is another important criterion for the evaluation of an SGS model. The friction coefficient is defined as

$$C_f = \frac{\mu \frac{\partial u}{\partial y}}{\frac{1}{2}\rho U_b^2}, \tag{33}$$

with U_b being the bulk velocity. Shown in Fig. 13 are distributions of the friction coefficients along the wall-normal direction predicted by SADSM(M), SADSM(F), and DSM at three different grid resolutions. It is seen that the curves for SADSM(M) and SADSM(F) almost collapse onto the DNS result. The results from DSM, however, deviate strongly from the DNS results, especially within the region of $y^+ < 12$. The DSM underpredicts the skin-friction coefficient, i.e., $C_f(y^+ = 0)$ by about 10% compared with the benchmark

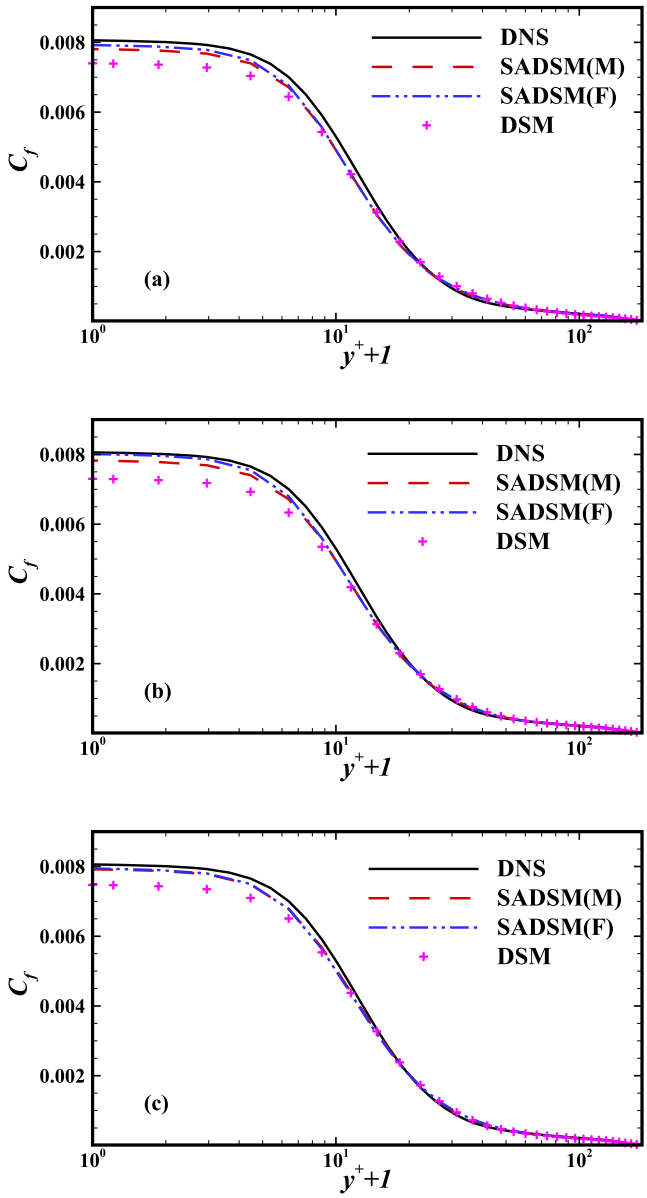

FIG. 13. Distributions of the friction coefficient along the wall-normal direction predicted by SADSM(M) (dashed line), SADSM(F) (dashed-double dotted line), and DSM (plus signs) at different grid resolutions: (a) GRID1 ($48 \times 64 \times 48$), (b) GRID2 ($64 \times 64 \times 64$), and (c) GRID3 ($80 \times 64 \times 80$). The DNS data (solid line) are plotted for comparison.

DNS result. The maximum deviation of the results given by SADSM(F) from the DNS benchmark data is about 1.5% at the lowest grid resolution (GRID1) used in this paper. Although the performance of SADSM(M) is not as good as that of SADSM(F) on GRID1 and GRID2, it is almost identical to the latter at the highest grid resolution (GRID3). It should be stressed that the traditional dynamic SGS model (including DSM) is proposed based on the scale-invariance assumption, in which the viscous effect is totally ignored. In the near-wall regions of wall-bounded turbulence, however, the viscous and inertia forces almost balance each other. Therefore, the viscous effect must be taken into account. The scale-adaptive SGS models proposed in this paper can effectively incorporate the viscous effect and are applicable for the multi-scale simulation of turbulence in the near-wall regions.

In order to evaluate the ability of the proposed models in predicting higher-Reynolds number turbulent channel flows, we have carried a series of simulations at $Re_\tau = 1000$. In Figs. 14(a) and 14(b), we display the mean velocity profile and the total Reynolds stress predicted by SADSM(M), SADSM(F), and DSM, respectively at $Re_\tau = 1000$. The DNS results from Lee and Moser[50] are also shown here for comparison. It can be seen in Fig. 14(a) that the mean velocity predicted by SADSM(M) and SADSM(F) is closer to the DNS profile than that given by DSM when $y^+ > 30$. From Fig. 14(b), we can also see that SADSM(M) and SADSM(F) can predict the total Reynolds stress more accurately than DSM in the region of $20 < y^+ < 300$.

To make a more comprehensive comparison, we have considered the Vreman model,[51] the volumetric strain-stretching (VSS) model,[52] and the explicit algebraic subgrid-scale stress model (EASSM)[53] as a supplement to DSM. Figs. 15(a) and 15(b) show the mean velocity profiles in wall units and the distributions of friction coefficients along the wall-normal direction at $Re_\tau = 180$ predicted by SADSM(M), SADSM(F), DSM, Vreman model, VSS model, and EASSM. All LESs are carried out on $80 \times 64 \times 80$ grid points. From Fig. 15(a), we can see that SADSM(M) and SADSM(F) predict the most accurate velocity profile if one takes the DNS data as reference. EASSM obtains a better result than DSM, VSS

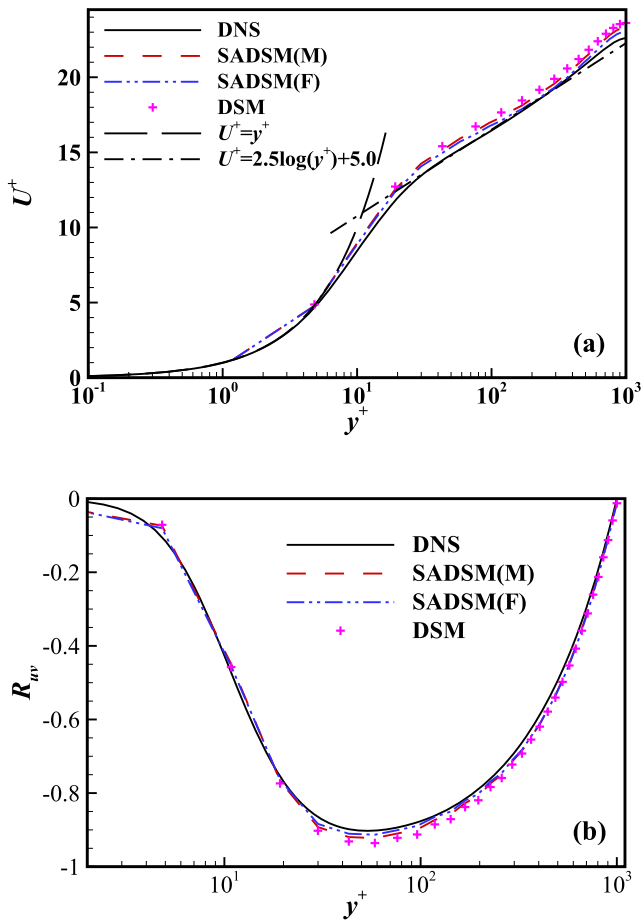

FIG. 14. (a) Mean velocity profiles in wall units and (b) total Reynolds stress predicted by SADSM(M) (dashed line), SADSM(F) (dashed-double dotted line), and DSM (plus signs) at $Re_\tau = 1000$. The DNS data from Lee and Moser[50] (solid line) are shown for comparison.

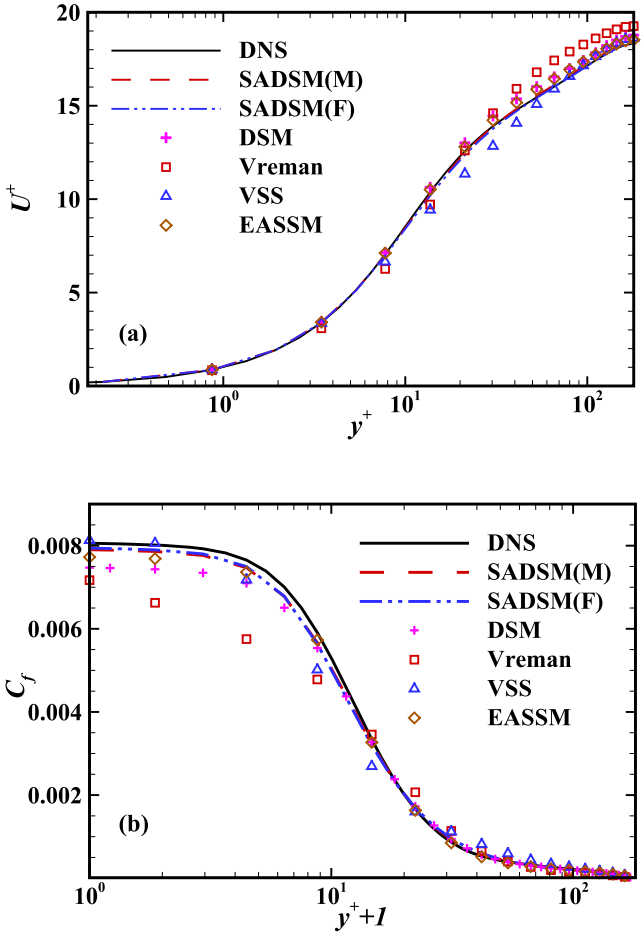

FIG. 15. (a) Mean velocity profiles in wall units, and (b) distributions of the friction coefficients along the wall-normal direction at $Re_\tau = 180$ predicted by SADSM(M) (dashed line), SADSM(F) (dashed-double dotted line), DSM (plus signs), Vreman model (squares), VSS model (deltas), and EASSM (diamonds) at grid resolution of $80 \times 64 \times 80$.

model, and Vreman model, although the VSS model performs quite well in the high-y^+ region. A similar conclusion can be drawn for the prediction of the friction coefficient as seen in Fig. 15(b). Although the performance of EASSM is close to that of the scale-adaptive models, SADSM(M) and SADSM(F) still make the most accurate predictions. The Vreman model underpredicts the friction coefficient severely when $y^+ < 10$.

As mentioned in Sec. II A, the ratio function of the dissipation rates (γ_Δ) derived based on homogeneous and isotropic turbulence also applies to flows with homogeneous directions. The corresponding SGS dissipation constraint can provide the SGS model with multiscale and scale-adaptive properties, which lead to the favourable results for turbulent channel flow as compared with other models considered in this paper. It is inferred that the proposed scale-adaptive models should offer a similar improvement in the simulation of turbulent flows with complex boundaries.

V. CONCLUSIONS

In this paper, the relation between the subgrid-scale (SGS) and resolved viscous dissipation rates of turbulent kinetic energy at an arbitrary filter scale ($\widetilde{\Delta}$) is investigated by using a hypothesized energy spectrum and a series of direct numerical simulation (DNS) data for incompressible isotropic turbulence. It turns out that the ratio ($\gamma_{\widetilde{\Delta}}$) of the SGS dissipation rate to the resolved viscous dissipation rate can be expressed as a function of the normalized filter length ($\widetilde{\Delta}/\eta$, with η being the Kolmogorov length scale) or the mesh Reynolds number ($Re_{\widetilde{\Delta}}$), and its variation with respect to $\widetilde{\Delta}/\eta$ (or $Re_{\widetilde{\Delta}}$) is almost independent of the Reynolds number.

The dissipation ratio factor $\gamma_{\widetilde{\Delta}}$ is then used as a grid self-recognizing constraint ($\beta_{\widetilde{\Delta}}$) for the model coefficients of dynamic Smagorinsky models. The SGS model with the model coefficient determined in such a manner is referred to as the scale-adaptive dynamic Smagorinsky model (SADSM). Specifically, the resultant models are called SADSM(M) and SADSM(F), respectively, if the dissipation ratio factor is given based on a model spectrum (17) and direct numerical simulation (DNS) data fitting (20). Furthermore, it is hypothesized that both of the coefficients in the mixed nonlinear SGS model also satisfy the same constraint as that in the single-term model. The corresponding dynamic mixed models are termed as SADMM(M) and SADMM(F), respectively.

The proposed scale-adaptive models are tested both *a priori* and *a posteriori* in simulations of homogeneous isotropic turbulence. In *a priori* text, the constraint parameter $\beta_{\widetilde{\Delta}}$ decreases monotonically with increasing mesh Reynolds number (or the filter width $\widetilde{\Delta}$), and approaches a sympototic value of 4. The calculated values for $\beta_{\widetilde{\Delta}}$ based on modeled and fitted $\gamma_{\widetilde{\Delta}}$ are all larger than that employed in the scale-dependent dynamic Smagorinsky model (SDDSM),[32] especially in the dissipative range. The model coefficients of the scale-adaptive models are found to be smaller than those of the conventional dynamic SGS models. In the *a posteriori* test, the scale-adaptive models can improve the accuracy in predicting the energy spectra at grid resolutions as compared with traditional dynamic models and SDDSM, especially on the dissipative-range grids. It is found that the use of the scale self-recognizing constraint can effectively optimize the allocation between the Smagorinsky part and the nonlinear part of the mixed SGS model, which is the major issue of the conventional dynamic mixed SGS models.

Then, the scale-adaptive models are tested *a posteriori* in the simulation of turbulent channel flow. It turns out that the scale-adaptive models can effectively incorporate the viscous effect in the near-wall region and obtain obviously better results for the mean velocity profile, the resolved turbulence intensities, the total Reynolds stress, skin-friction coefficient, etc.

It should be stressed that the constraint parameter introduced in the present paper can be straightforwardly incorporated in optimizing any other base models, such as stretched vortex model and anisotropic model, in both Eulerian and Lagrangian dynamic regimes.

ACKNOWLEDGMENTS

We are grateful to Weidong Su and Yipeng Shi for many useful discussions on this work. Numerical simulations were finished on the Tianhe-1A supercomputing facility at National Supercomputer Center in Tianjin, China. We acknowledge the financial support provided by National Natural Science

Foundation of China (Grant Nos. 11472278, 11372007, 91441103, and 11372330). This work was also funded by the National Key Research and Development Program of China (Grant No. 2016YFA0401200).

[1]J. W. Deardorff, "A numerical study of three-dimensional turbulent channel flow at large Reynolds numbers," J. Fluid Mech. **41**, 453–480 (1970).
[2]D. J. Hill, C. Pantano, and D. I. Pullin, "Large-eddy simulation and multi-scale modelling of a Richtmyer-Meshkov instability with reshock," J. Fluid Mech. **557**, 29–61 (2006).
[3]P. J. Mason, "Large-eddy simulation of the convective atmospheric boundary layer," J. Atmos. Sci. **46**, 1492–1516 (1989).
[4]F. Porté-Agel, C. Meneveau, and M. B. Parlange, "A scale-dependent dynamic model for large-eddy simulation: Application to a neutral atmospheric boundary layer," J. Fluid Mech. **415**, 261–284 (2000).
[5]J. W. Deardorff, "The use of subgrid transport equation in a three dimensional model of atmospheric turbulence," J. Fluid Eng. **95**, 429–438 (1973).
[6]M. Germano, "Turbulence: The filtering approach," J. Fluid Mech. **238**, 325–336 (1992).
[7]V. Borue and S. Orszag, "Local energy flux and subgrid-scale statistics in three-dimensional turbulence," J. Fluid Mech. **336**, 1–31 (1998).
[8]Z. Xiao, M. Wan, S. Chen, and G. L. Eyink, "Physical mechanism of the inverse energy cascade of two-dimensional turbulence: A numerical investigation," J. Fluid Mech. **619**, 1–44 (2009).
[9]C. P. Yu, Z. Xiao, and X. L. Li, "Dynamic optimization methodology based on subgrid-scale dissipation for large eddy simulation," Phys. Fluids **28**, 015113 (2016).
[10]M. Lesieur and O. Métais, "New trends in large eddy simulations of turbulence," Annu. Rev. Fluid Mech. **28**, 45–82 (1996).
[11]U. Piomelli, "Large-eddy simulation: Achievements and challenges," Prog. Aerosp. Sci. **35**, 335–362 (1999).
[12]C. Meneveau and J. Katz, "Scale-invariance and turbulence models for lage-eddy simulation," Annu. Rev. Fluid Mech. **32**, 1–32 (2000).
[13]U. Piomelli and E. Balaras, "Wall-layer models for large-eddy simulations," Annu. Rev. Fluid Mech. **34**, 349–374 (2002).
[14]J. Smagorinsky, "General circulation experiments with primitive equation," Mon. Weather Rev. **91**, 99–164 (1963).
[15]D. K. Lilly, "On the application of the eddy viscosity concept in the inertial sub-range of turbulence," NCAR MS 123, National Centre for Atmospheric Research, Boulder, CO, 1966.
[16]D. K. Lilly, "The representation of small-scale turbulence in numerical simulations," in *Proceedings of the IBM Scientific Computing Symposium on Environmental Sciences* (IBM Data Processing Division, White Plains, NY, 1967), pp. 195–209.
[17]O. J. McMillan, J. H. Ferziger, and R. S. Rogallo, "Test of new subgrid scale models in strained turbulence," AIAA Paper No. 80-1339, 1980.
[18]P. Moin and J. Kim, "Numerical investigation of turbulent channel flow," J. Fluid Mech. **118**, 341–377 (1982).
[19]E. R. Van Driest, "On turbulent flow near a wall," J. Aeronaut. Sci. **23**, 1007–1011 (1956).
[20]M. Germano, U. Piomelli, P. Moin, and W. Cabot, "A dynamic subgridscale eddy viscosity model," Phys. Fluids A **3**, 1760–1765 (1991).
[21]S. Ghosal, T. S. Lund, P. Moin, and K. Akselvoll, "A dynamic localization model for large-eddy simulation of turbulent flows," J. Fluid Mech. **286**, 229–255 (1995).
[22]C. Meneveau, T. S. Lund, and W. Cabot, "A Lagrangian dynamic subgrid-scale model of turbulence," J. Fluid Mech. **319**, 353–389 (1996).
[23]D. K. Lilly, "A proposed modification of the Germano subgrid-scale closure method," Phys. Fluids A **4**, 633–635 (1992).
[24]S. Liu, C. Meneveau, and J. Katz, "Experimental study of similarity subgrid-scale models of turbulence in the far-field of a jet," Appl. Sci. Res. **54**, 177–190 (1995).
[25]Y. Zang, R. L. Street, and J. Koseff, "A dynamic mixed subgrid-scale model and its application to turbulent recirculating flows," Phys. Fluids A **5**, 3186–3196 (1993).
[26]B. Vreman, B. Geurts, and H. Kuerten, "Large eddy simulation of the turbulent mixing layer," J. Fluid Mech. **339**, 357–390 (1997).
[27]D. Fauconnier and E. Dick, "Analytical and numerical study of resolution criteria in large-eddy simulation," Phys. Fluids **26**, 065104 (2014).
[28]C. Ronchi, M. Ypma, and V. M. Canuto, "On the application of the Germano identity to subgrid-scale modeling," Phys. Fluids A **4**, 2927–2929 (1992).
[29]P. Voke, "Subgrid-scale modelling at low mesh Reynolds number," Theor. Comput. Fluid Dyn. **8**, 131–143 (1996).
[30]Z. Y. Yang and P. R. Voke, "Large-eddy simulation studies of bypass transition," in *Engineering Turbulence Modelling and Experiments 2*, edited by W. Rodi and F. Martelli (Elsevier, Amsterdam, 1993), pp. 603–611.
[31]C. Meneveau and T. S. Lund, "Dynamic model with scale-dependent coefficients in the viscous range," in *Proceedings of the 1996 Summer Program* (Center for Turbulence Research, Stanford University, 1996), pp. 275–290.
[32]C. Meneveau and T. S. Lund, "The dynamic Smagorinsky model and scale dependent coefficients in the viscous range of turbulence," Phys. Fluids **9**, 3932–3934 (1997).
[33]E. Bou-Zeid, C. Meneveau, and M. Parlange, "A scale-dependent Lagrangian dynamic model for large eddy simulation of complex turbulent flows," Phys. Fluids **17**, 025105 (2005).
[34]C. Meneveau, "Statistics of turbulence subgrid-scale stresses: Necessary conditions and experimental tests," Phys. Fluids **6**, 815–833 (1994).
[35]Y. Shi, Z. Xiao, and S. Chen, "Constrained subgrid-scale stress model for large eddy simulation," Phys. Fluids **20**, 011701 (2008).
[36]C. P. Yu and Z. Xiao, "Refined subgrid-scale model for large-eddy simulation of helical turbulence," Phys. Rev. E **87**, 013006 (2013).
[37]C. P. Yu, Z. Xiao, Y. Shi, and S. Chen, "Joint-constraint model for large-eddy simulation of helical turbulence," Phys. Rev. E **89**, 043021 (2014).
[38]S. Chen, Z. Xia, S. Pei, J. Wang, Y. Yang, Z. Xiao, and Y. Shi, "Reynolds-stress-constrained large-eddy simulation of wall-bounded turbulent flows," J. Fluid Mech. **703**, 1–28 (2012).
[39]C. Meneveau, "Germano identity-based subgrid-scale modeling: A brief survey of variations on a fertile theme," Phys. Fluids **24**, 121301 (2012).
[40]S. B. Pope, *Turbulent Flows* (Cambridge University Press, 2000).
[41]L. S. G. Kovasznay, "Spectrum of locally isotropic turbulence," J. Aeronaut. Sci. **15**, 745–753 (1948).
[42]S. A. Orszag and G. S. Patterson, "Numerical simulation of three-dimensional homogeneous isotropic turbulence," Phys. Rev. Lett. **28**, 76 (1972).
[43]S. Y. Chen, G. D. Doolen, R. H. Kraichnan, and Z. S. She, "On statistical correlations between velocity increments and locally averaged dissipation in homogeneous turbulence," Phys. Fluids A **5**, 458–463 (1993).
[44]S. Liu, C. Meneveau, and J. Katz, "On the properties of similarity subgrid-scale models as deduced from measurements in a turbulent jet," J. Fluid Mech. **275**, 83–119 (1994).
[45]R. Anderson and C. Meneveau, "Effects of the similarity model in finite-difference LES of isotropic turbulence using a Lagrangian dynamic mixed model," Flow, Turbul. Combust. **62**, 201–225 (1999).
[46]K. R. Sreenivasan, "On the universality of the Kolmogorov constant," Phys. Fluids **7**, 2778 (1995).
[47]P. K. Yeung and Y. Zhou, "On the universality of the Kolmogorov constant in numerical simulations of turbulence," Phys. Rev. E **56**, 1746–1752 (1997).
[48]J. Kim, P. Moin, and R. D. Moser, "Turbulent statistics in fully developed channel flow at low Reynolds number," J. Fluid Mech. **177**, 133–166 (1987).
[49]C. Canuto, C. Hussaini, M. Y. Quarteroni, and T. A. Zang, *Spectral Methods in Fluid Dynamics* (Springer, 1988).
[50]M. Lee and R. D. Moser, "Direct numerical simulation of turbulent channel flow up to $Re_\tau = 5200$," J. Fluid Mech. **774**, 395 (2015).
[51]A. W. Vreman, "An eddy-viscosity subgrid-scale model for turbulent shear flow: Algebraic theory and applications," Phys. Fluids **16**, 3670 (2004).
[52]S. Ryu and G. Iaccarino, "A subgrid-scale eddy-viscosity model based on the volumetric strain-stretching," Phys. Fluids **26**, 065107 (2014).
[53]A. Rasam, S. Wallin, G. Brethouwer, and A. V. Johansson, "Large eddy simulation of channel flow with and without periodic constrictions using the explicit algebraic subgrid-scale model," J. Turbul. **15**, 752 (2014).